EMPIR
EURAMET
The EMPIR initiative is co-funded by the European Union's Horizon 2020 research and innovation programme and the EMPIR Participating States

14IND10 MET5G D4

Evaluation report on comparing SINR performance between measurement campaigns, verifying and applying changes to SINR definition for 5G communication

Project Number: JRP 14IND10

Project Title: Metrology for 5G Communications (MET5G)

Document Type: Evaluation Report

Authors: Tian Hong Loh, David Cheadle, Tim Brown, Thomas Eriksson, Koen Buisman, and Michael Dieudonne

Lead Partner: NPL

Participating Partners: Chalmers, SURREY, Keysight DK

Due Date: March 2018

Submitted Date: April 2018

NPL National Physical Laboratory
CZECH METROLOGY INSTITUTE
RI SE
CHALMERS UNIVERSITY OF TECHNOLOGY
UNIVERSITY OF SURREY
KEYSIGHT TECHNOLOGIES
Anritsu envision:ensure

Table of Contents

1 Scope of the document 3
2 Introduction 3
2.1 Background 3
2.2 Measurement Campaign (1) introduction 4
2.2.1 Hardware 4
2.2.2 Measurement setup and test scenarios 6
2.2.3 Measurement details 8
2.3 Measurement Campaign (2) introduction 8
2.3.1 Hardware 8
2.3.1.1 Chalmers mm-wave MIMO testbed 8
2.3.1.2 NPL mm-wave MIMO testbed 10
2.3.2 Measurement setup 11
2.3.3 Measurement details 12
3 Feedback of findings to simulator development 13
3.1 Using MATE and the MATE simulator 13
3.2 5G Candidate Waveform Generation and Analysis 14
3.2.1 5G Candidate Waveform 14
3.2.2 Waveform generation 15
3.2.3 Waveform analysis 15
3.3 Measurement and Simulation setups 16
3.4 Comparison between MATE and the MATE Simulator 17
3.4.1 Measurements with a calibrated simulator 18
3.4.2 Investigation on MATE simulator channel model 20
3.4.3 Comparison for Constellation Diagram and Received Spectrum 21
3.4.4 Investigation on adjustments to the simulator noise floor 22
3.5 Further investigations using the MATE simulator 23
3.5.1 Carrier frequency offset 23
3.5.2 Synchronisation failure 23
3.5.3 Investigation on an in-band interference source 24
3.5.4 Investigation on an out-of-band interference source 25
4 Analysis of data findings and Verification of the SINR definition 27
4.1 Measurement Campaign (1) 27
4.2 Measurement Campaign (2) 29
5 Conclusion 32
6 References 32

Glossary

5G	Fifth-generation wireless network
ADC	Analog-to-Digital Converter
AGC	Automatic Gain Control
BER	Bit Error Rate
BPF	Band Pass Filter
BPSK	Binary-Phase-Shift-Keyed
CFO	Carrier Frequency Offset
CP-OFDM	Cyclic-Prefix Orthogonal Frequency Division Multiplexing (CP-OFDM)
DAC	Digital-to-Analog Converters
EVM	Error Vector Magnitude
FPGA	Field-Programmable Gate Arrays
IF	Intermediate Frequency
LNA	Low Noise Amplifier
LO	Local Oscillator
LTE	Long-Term Evolution
MATE	Massive MIMO Testbed (developed by Chalmers)
MIMO	Multiple-Input-Multiple-Output
mm-wave	Millimeter wave
NR	New Radio
QAM	Quadrature Amplitude Modulation
QPSK	Quadrature Phase Shift Keying
RF	Radio Frequency
RMS	Root Mean Square
Rx	Receiving
SDR	Software Defined Radio
SINR	Signal-to-Interference-plus-Noise Ratio
SISO	Single-Input-Single-Output
TDM	Time Division Multiplex
Tx	Transmitting
VST	Vector Signal Transceiver

1 Scope of the document

This document, namely, Deliverable 4 (D4), serves as an evaluation report on comparing signal-to-interference-plus-noise-ratio (SINR) performance for measurement campaigns (1) and (2) (i.e. work carried out, respectively, from WP1 under Task 1.2 and from WP2 under Task 2.2), feedback to software simulator development in Task 2.1, verifying and applying changes to SINR definition for 5G communication, where applicable.

In this work, MIMO communications were considered. Three multiple-input-multiple-output (MIMO) testbeds (2 × 2 mm-wave MIMO, 8 × 2 mm-wave MIMO, and 32 × 3 sub-6GHz massive MIMO) have been used. The aim is to compare and analyses the SINR measured results between the measurement campaigns for: 1) in-band; and 2) out-of-band scenarios. This will help ascertain the strengths and weaknesses of each definition.

A 5G waveform candidate is employed. This work enables determination of possible points of weakness for potential future 5G system. Several measurement campaigns have been performed by NPL, Chalmers and SURREY. Based on the measurement findings, the SINR definition is reviewed in this report.

2 Introduction

2.1 Background

It is expected that the measurement campaign (1) in A1.2.3 will show some results that are not predicted by theory or by the synthetic setup used for the measurement campaign (2) in Task 2.2. The objective of this task is therefore to explore the underlying causes to discrepancies in the results. The results will enable updating the activities in task 2.2, and further refinement of the SINR definition(s) in WP1.

Accordingly to 14IND10 JRP, the activities covered under this report are:

- NPL and Chalmers will perform an analysis of data findings from the measurement campaign (1) in A1.2.3 and measurement campaign (2) in A2.2.4, and comparison with the results as given in A2.2.1 and A2.2.2.
- NPL and Chalmers will provide feedback of findings to simulator development in Task 2.1, activity A2.1.7 in order to improve the simulator output.
- NPL and Chalmers will verify the SINR definition using the testbed system developed in Task 2.1 with a defined controllable sounding environment.
- NPL and Chalmers will use output from A2.3.3 to apply changes to definition of SINR determined in WP1 A1.1.3, and feed back to A1.3.3 in WP1

The following provides the SINR definition derived from technical reports written under WP1 activities – A1.1.3 [1] for MIMO:

$$\mathrm{SINR} = \frac{\overline{|h_{\mathrm{w}}(t)|}^2}{A_{\mathrm{i1}}\overline{|h_{\mathrm{i1}}(t)|}^2 + A_{\mathrm{i2}}\overline{|h_{\mathrm{i2}}(t)|}^2 + \sigma_{\mathrm{n}}^2} \tag{1}$$

where $h_{\mathrm{w}}(t)$ is the propagation channel of the desired signal, $h_{\mathrm{i}}(t)$ is the propagation channel of

the interfering signal, A_i is the relative attenuation of the interferer controlled by a step attenuator and σ_n^2 is the mean noise power of the additive Gaussian noise. The subscripts of 1 are for the first interferer and 2 for the second.

As shown in the D1 validation report [2], a relationship can be made between the linear SINR and the EVM as follows:

$$\mathrm{EVM}(\%) = \frac{A}{\sqrt{\mathrm{SINR}}} \tag{2}$$

where the value of the gradient, determined by A is highly dependent on the QAM order. The value of A for up to three interferers and for each QAM is shown in Table 1. Note that this assumes a frequency flat channel and no nonlinear effects at the transmitter, which in a real system would have to be accounted for.

Table 1 - Comparison of the gradient value for the log linear relationship between EVM and SINR for differing QAM order and up to three interferers (Ints) in a frequency flat channel.

QAM Order	A (1 Int)	A (2 Ints)	A (3 Ints)
8	65	77	77
16	73	78	78
32	88	90	92
64	107	107	107
128	115	115	115
256	129	129	129
512	140	140	140

2.2 Measurement Campaign (1) introduction

This section gives a short overview and introduction of a typical configuration of the sub-6GHz massive MIMO testbed at SURREY with the associated measurement setup using the MIMO antenna developed under A1.2.2. The antenna was designed to analyse the impact of angular separation of antenna patterns against spatial separation using commercially available omnidirectional antennas.

2.2.1 Hardware

SURREY owns a Propsound wideband MIMO channel sounder, which has the ability to measure wideband MIMO channels of up to 56×32 transmitting (Tx) and receiving (Rx) elements at frequencies from 2.2 – 2.6 GHz and 5.2 – 5.4 GHz at null-to-null bandwidths of up to 200 MHz. It transmits a direct-sequence spread spectrum signal, produced from binary-phase-shift-keyed (BPSK) modulated pseudo-noise codes, which will ascertain the wideband impulse response from evaluating the correlation of the pseudo-noise codes.

The channel sounder has one transmit box with architecture shown in Figure 1 (a) and a receive architecture shown in Figure 1 (b), which are controlled by a laptop computer. Each MIMO channel is obtained sequentially by using fast switching time division multiplex (TDM) techniques, where around three MIMO channel matrices should be captured in each wavelength, with each MIMO

matrix remaining well within the channel coherence time. Thus there is a suitable minimum level of sampling to capture the data.

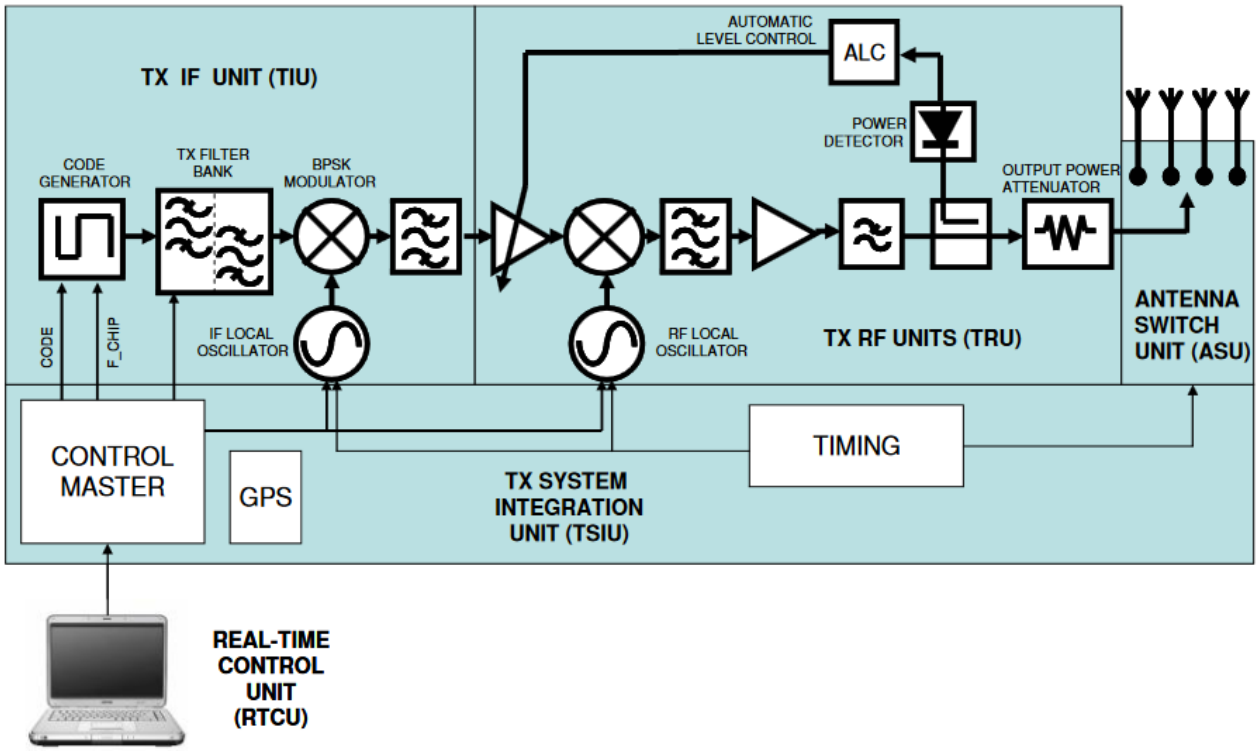

(a)

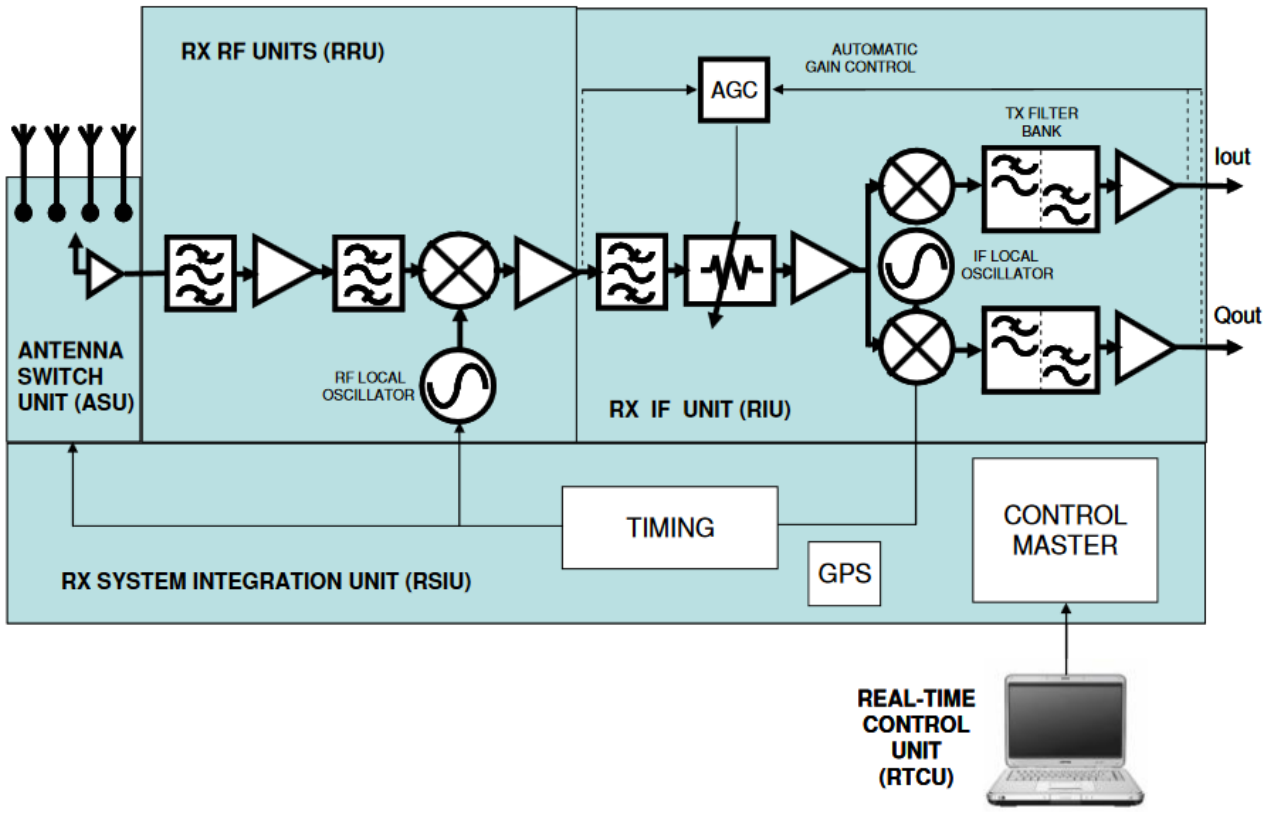

(b)

Figure 1 Diagram of the architecture of the Propsound Channel Sounder at the (a) transmit and (b) receive end.

The transmitter works by means of a two-stage up conversion with two local oscillators (LOs), one at intermediate frequency (IF) then the second at radio frequency (RF) with appropriate band pass filters (BPFs) at each output. A power amplifier then outputs to the transmit antennas, with a pad attenuator and level detector to provide automatic level control feedback. A timing device will then appropriately set the switching sequence. The reverse process with a superheterodyne architecture using an analog-to-digital converter (ADC) happens to generate IQ at baseband. Automatic gain control (AGC) is used to keep small scale fading within the ADC dynamic range. A low noise amplifier (LNA) is positioned inside the antenna switch unit enclosure to minimize receiver noise figure.

2.2.2 Measurement setup and test scenarios

The wideband channel sounder setup was configured to undertake 32×6 MIMO channel measurements over a 200 MHz bandwidth (of which 120 MHz was used for evaluation) at 2.4 GHz. Therefore it was possible to conduct two 32×3 massive MIMO measurements simultaneously as it is required to have greater than ten times the number of elements at the transmitter than the number of single antenna receivers to meet the criteria [3]. The measurement was carried out in an outdoor obstructed line of sight environment with significant vegetation to enable some channel fading but varying separation of beam space between the three receivers as illustrated in Figure 2 as a plan view with a photograph of the environment in Figure 3.

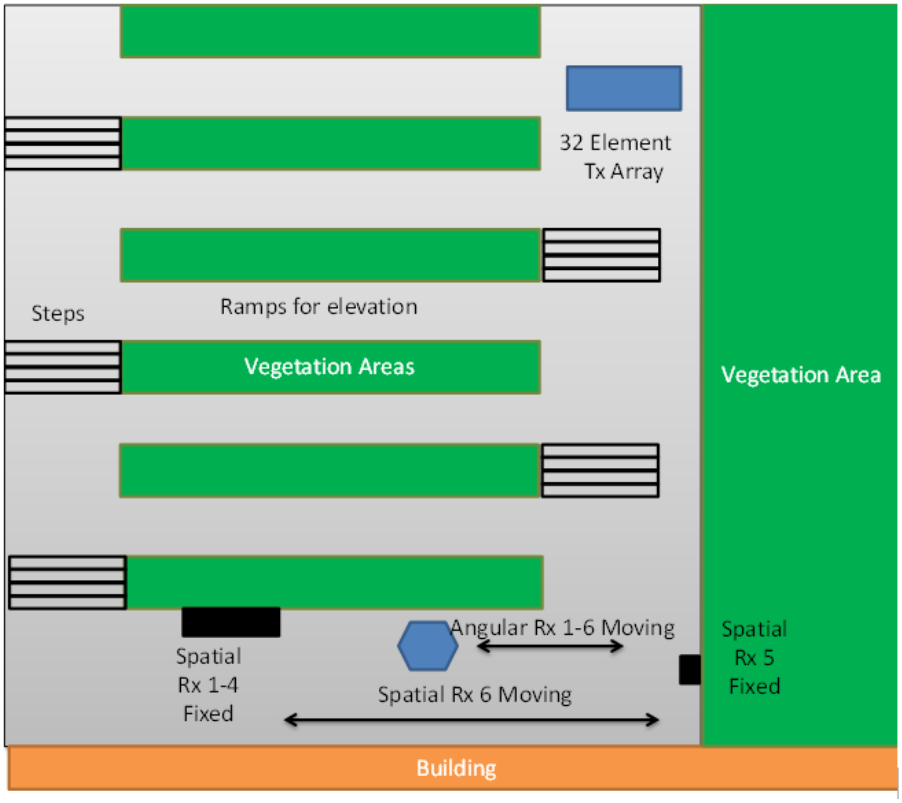

Figure 2 Plan view of the outdoor massive MIMO measurement area including two setups for Rx 1-6, spatial and angular.

(a)

(b)

(c)

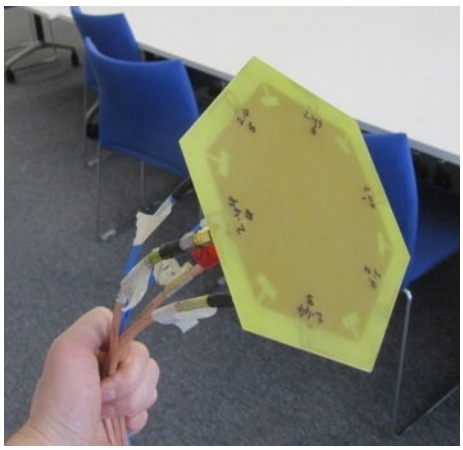

(d)

Figure 3 Photographs of the measurement environment showing the 32 element transmit array and (a) Rx1 to Rx4 at a fixed position and (b) Rx6 moving. Antennas used show close up views of (c) Rx1 to Rx4 in the spatial case and (d) Rx1 to Rx6 in the angular case.

The transmit array consisted of 32 dual polar patch elements, while the receiver antennas Rx1 to Rx6 were commercial omnidirectional monopole antennas with a small ground plane attached to them. For the first set of 32×3 data in the spatial case, Rx1 to Rx3 were used, where their close proximity, stationarity and fixed position as shown in Figure 3(c) and indicated in Figure 2 would create substantial interference thus limiting SINR. For the second set of 32×3 data, in the spatial case, Rx4 and Rx5 are separated widely as shown in Figure 2, which will allow some beam separation to improve SINR between the two antennas. Rx6 in the spatial on the other hand is moved back and forth horizontally as indicated in Figure 2. The results for Rx6 in the spatial case are interesting to analyze as they will determine how reliably SINR can be tracked as the channel state changes dynamically.

For angular measurements using the angular antenna, the cables for Rx1 through to Rx6 were disconnected and then connected to a six element inverted-F antenna shown in Figure 3(d) indicated also in Figure 2 as a hexagon, which was moved horizontally in the measurement. Therefore two sets of 32×3 angular measurements could be undertaken to evaluate how angular separation affected SINR.

2.2.3 Measurement details

Measurements were carried out lasting approximately 20 seconds, where the sample to sample time period was 36.56 ms corresponding to a 27.35 Hz sampling rate. This was selected as it was found to be more than three times the maximum Doppler frequency at a walking speed of 4 km/h, which was 8.89 Hz. Hence the coherence time of the channel could be sufficiently determined, while any possibility of aliasing regarding the second order channel statistics was avoided. The channel impulse responses were measured and stored for post processing. There are three different scenarios of SINR that were analysed in this study from three different receivers:

Rx3 Spatial – In this situation the receiver was stationary but in close spatial separation to two other receivers which would cause substantial interference from the downlinks to those receivers formed by zero forcing. Therefore this would make a substantially low SINR that is largely static, only changing due to moving scatterers.

Rx6 Spatial – This receiver was moving, while the two other receivers causing interference from the transmitted modes to those receivers using zero forcing would be highly time variant and also frequency selectivity at each time interval would change.

Rx 3 Angular – This receiver was connected to the angular antenna formed in A1.1.2 and the interference was substantially impacted by having the other two receivers close to it but also there was significant time variant effects as the angular effects changed in each time slot.

2.3 Measurement Campaign (2) introduction

This section gives a short overview and introduction of a typical configuration of the mm-wave MIMO testbeds at Chalmers and NPL with the associated measurement setup and the associated considered scenarios.

2.3.1 Hardware

Two complementary MIMO metrology testbeds (one 2×2 MIMO at NPL and another one 8×2 MIMO at Chalmers) have been developed and tested for millimetre-wave (mm-wave) operation [4]. Both the mm-wave testbeds could be divided into three parts: (1) baseband hardware; (2) software and (3) RF frontend hardware. The full details is provided in [4].

2.3.1.1 Chalmers mm-wave MIMO testbed

The 8×2 Chalmers mm-wave MIMO testbed has been made available by remote access. Some key features of the testbed are summarized in Table I. A schematic is given in Figure 4.

TABLE I. KEY FEATURE OF THE MATE TESTBED

	MATE
Operating frequency	28 – 31 GHz
Analog Bandwidth per TX/RX chain	1 GHz
No. TX	8 (extendable to 16)
No. RX	1 or 2 (extendable to 9)
No. FPGAs (Field-Programmable Gate Arrays)	18
RF Output power per TX chain	Max. -4 dBm
Noise figure RX	3 dB[a]

[a] From datasheet

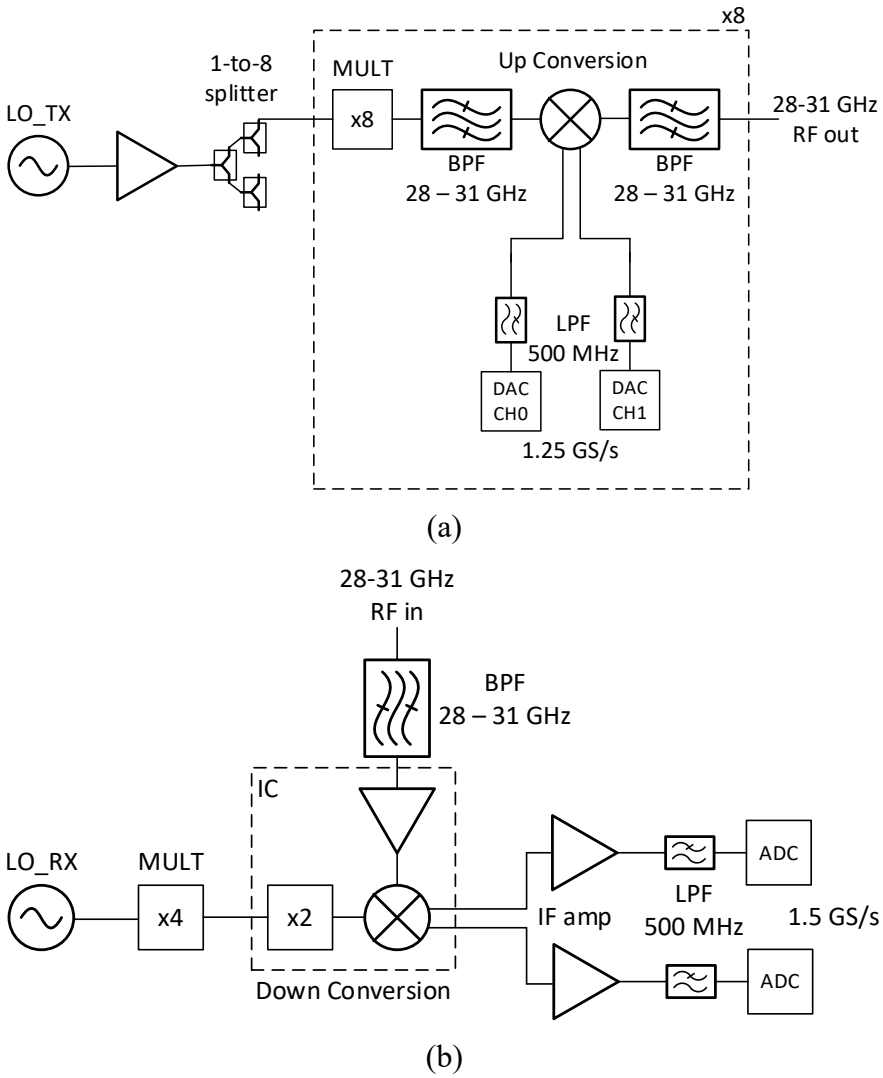

Figure 4 Schematic overview: (a) MATE transmitter; (b) MATE receiver. Note that only one of eight upconverting branches is shown.

The RF hardware is constructed from off-the-shelf components, supports >1 GHz analog bandwidth and operates between 28 – 31 GHz. To enable digital beamforming and MIMO signal processing, each TX chain of the system has to be coherent with respect to the other TX chains. To reach this goal we distribute a ~3.5 - 3.875 GHz local oscillator (LO) signal to each of the TX chains (Figure

4), where the LO is subsequently multiplied by a factor of 8. This choice was made to avoid the need to distribute ~30 GHz LO signals. An LO amplifier at ~3.5 GHz is used to compensate for the losses in distributing the LO. Note that if there is more than one RX, we employ a similar LO distribution for the RX as well. Unwanted products arising from the LO multipliers are suppressed with coupled stripline bandpass filters, after which the LO signals drive IQ modulators, where the baseband I and Q signals are provided by 1.25 GS/s digital-to-analog converters (DACs). After the IQ modulator a second identical bandpass filter is applied. The signal here can be connected to an antenna, as is the case in the configuration as discussed in this paper. To allow for larger distances, a power amplifier can be inserted.

The RX chain is similar to the TX chains, one exception is that we use a direct IQ downconverter IC with integrated x2 LO multiplier. Thus the LO multiplier we have constructed is x4. The downconverter IC contains a low noise amplifier and gives out the down-converted I and Q, which are subsequently amplified, filtered and digitized by 1.5 GS/s ADCs.

2.3.1.2 NPL mm-wave MIMO testbed

The 2×2 NPL mm-wave MIMO testbed is capable of performing spatial diversity MIMO transmission. Some key features of the testbed are summarized in Table II. The schematics for transmitting (Tx) and receiving (Rx) ends are given in Figure 5 and Figure 6, respectively.

TABLE II. KEY FEATURE OF THE NPL TESTBED

	NPL
Operating frequency	27.5 – 31 GHz
Analog Bandwidth per TX/RX chain	80 MHz
No. TX	2 (extendable to 4)
No. RX	2 (extendable to 4)
No. FPGAs	4

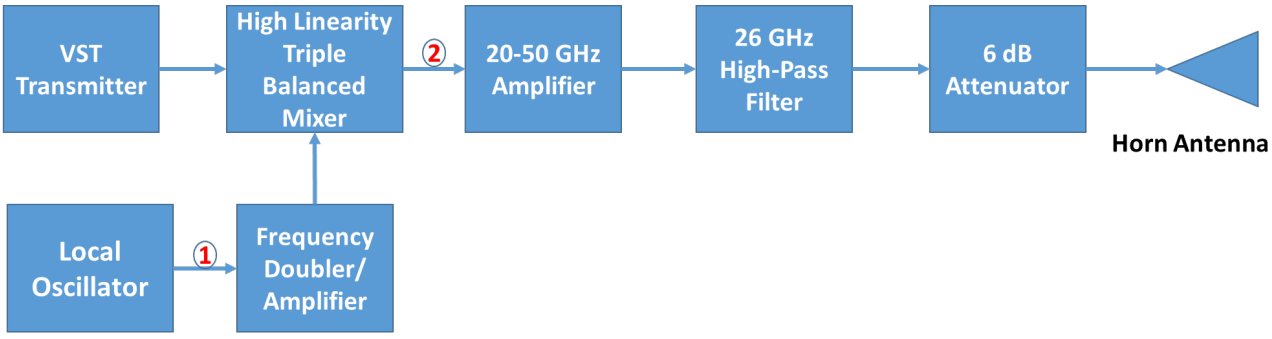

Figure 5 Single-channel layout for the transmit-end of the MIMO system.

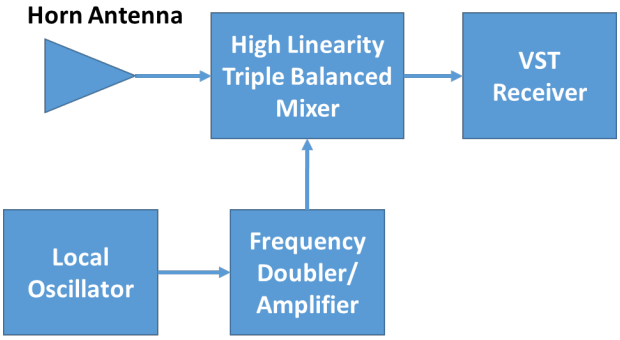

Figure 6 Single-channel layout for the receive-end of the MIMO system.

This testbed was built using two vector signal transceiver (VST) system modules with a real-time signal processing software defined radio (SDR) capability, two pairs of standard gain horns at the transmit and receive ends and frequency up and down conversion hardware. The VST modules are acting as baseband part of the MIMO system and have a frequency coverage from 65 MHz to 6 GHz. Providing a suitable filter is chosen to limit spurious output, the system is envisaged capable of operating with RF frequency range from 20.65 GHz up to 46 GHz. In initial work carried out in, the LO and IF frequencies were chosen to be 25 GHz and 5 GHz, respectively, to operate the system at RF of 30 GHz. Signal generation and measurement is performed using a pair of sub-6 GHz VSTs. The MIMO decoder uses the measured IQ data at the receivers, and previously obtained channel state information in the form of a measured H-matrix, to recover two simultaneously transmitted frames.

2.3.2 Measurement setup

This section details measurements made with both 5G mm-wave MIMO testbeds co-located, after the NPL system was moved to Chalmers (see Figure 7).

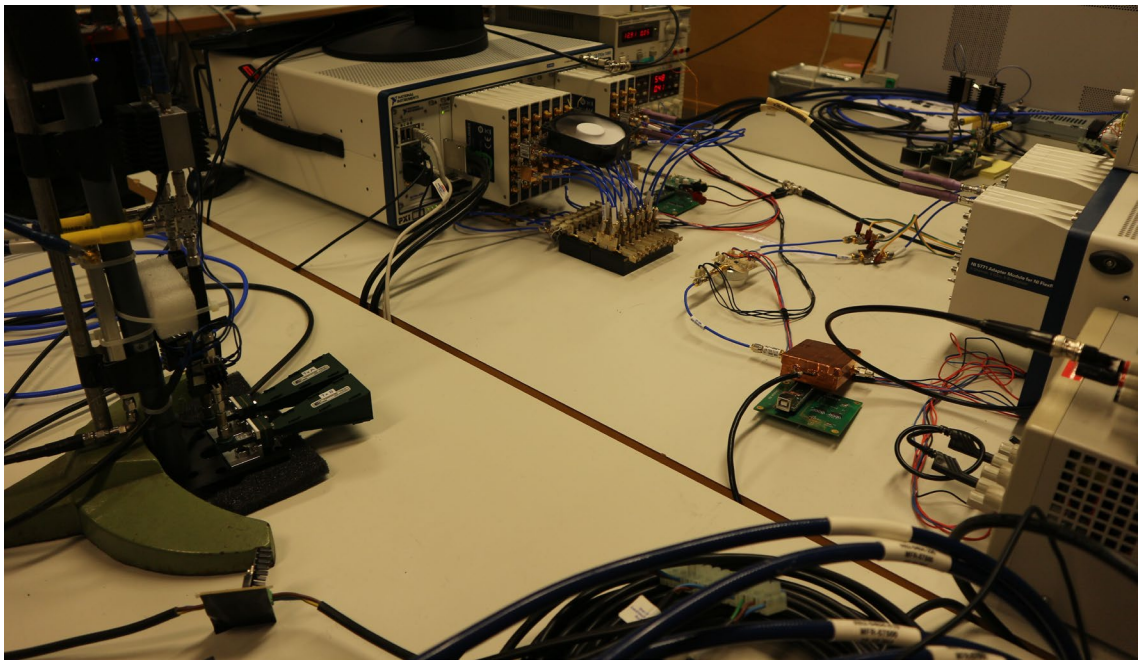

Figure 7 Photograph of MATE and NPL testbeds set up at Chalmers. MATE is visible at the centre of the photograph and the NPL transmit and receive antennas are visible in the lower left and upper right corners of the photograph respectively.

2.3.3 Measurement details

A series of measurements were made with both testbeds transmitting and receiving with all available antennas was conducted. This is to assess SINR, with the MATE system acting as the desired signal and the NPL acting as an interference source. Both systems were setup to operate at a center frequency of 28.5 GHz.

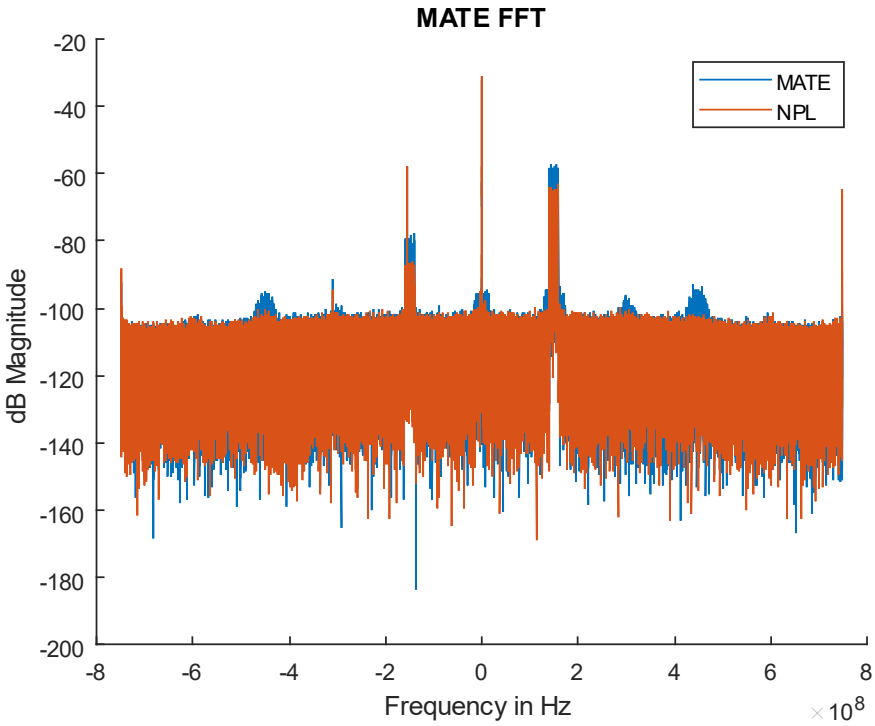

(a)

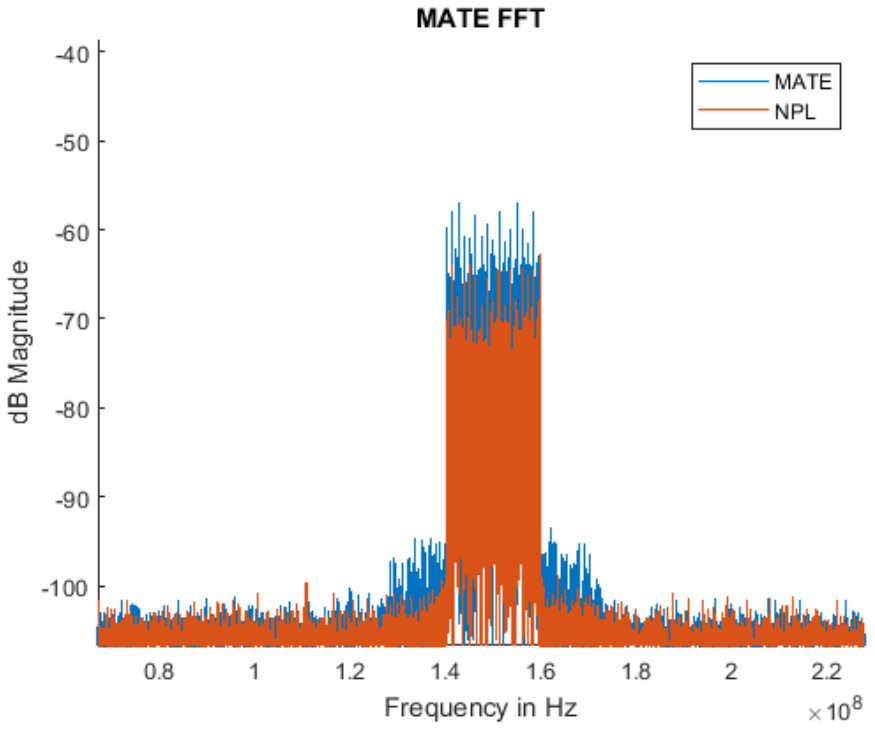

(b)

Figure 8 A comparison of a snapshot of the frequency spectrum acquired by the MATE receiver when either MATE or NPL system was transmitting: (a) The complete spectrum and (b) the spectrum zoomed to the region of interest are displayed. The region of interest is offset by + 150 MHz from the MATE centre frequency due to the steps performed in the MATLAB code described previously.

The control software for the NPL system, which generates and decode the 5G candidate waveforms, was modified to allow it to control MATE. Frequency alignment was performed by alternating between transmitting using MATE or the NPL system and converting the IQ data recorded by MATE to a frequency domain plot. The IF frequency of the NPL system was adjusted to align the two systems.

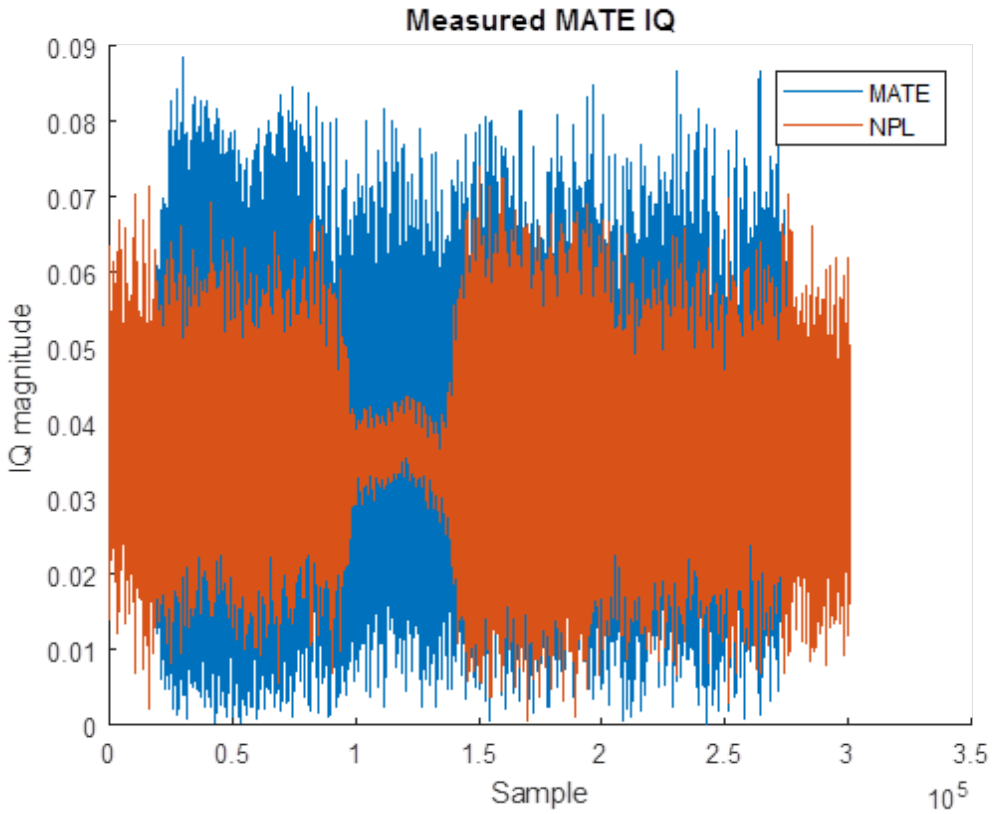

Figure 9 Magnitude of time domain IQ data recorded by the MATE receiver when both MATE and NPL system were transmitting. The position of the NPL interference signal will change for each measurement as the two systems are not synchronized.

For the measurements with NPL as the interference source, before automated SINR measurements were made a series of initial measurements were conducted. Figure 8 shows a comparison of a snapshot of the frequency spectrum acquired by the MATE receiver when either MATE or the NPL system was operating in single-input-single-output (SISO) mode. The IQ data from the MATE receiver was captured and stored to file during these initial runs (see Figure 9), the data was later processed and used to ensure that MATE and NPL systems were transmitting at the same time and in the same frequency band.

3 Feedback of findings to simulator development

This section provides the feedback of findings to Chalmers' simulator development. A comparison of the mm-wave Massive MIMO testbed (MATE) hardware at Chalmers and its simulator, entitled 'MATE simulator' and several investigations over the system parameters are performed.

3.1 Using MATE and the MATE simulator

The MATE client software allows a user to upload IQ data to MATE for transmission. The details

on how to use the MATE system has been provided in [4]. The client supports transmission using a number of configuration modes. One of these modes is a simulator which uses a software model to simulate the performance of the MATE hardware.

The simulator is supplied with the MATE client code and is activated by passing the simulate parameter when creating the c_mate object. When simulate is not specified the physical MATE hardware is used for the measurement. Examples of the commands used to interface with MATE and the simulator are shown in Table 1.

Table 2 Commands used to activate MATE or the MATE simulator

Condition	Example command
MATE	`c_mate('calibrate','sync');`
MATE simulator	`c_mate('simulate','calibrate','sync');`

3.2 5G Candidate Waveform Generation and Analysis

3.2.1 5G Candidate Waveform

Testing was performed on MATE and the MATE simulator using a Cyclic-Prefix Orthogonal Frequency Division Multiplexing (CP-OFDM) waveform, the same waveform chosen for 5G new radio (NR) (see Figure 10 [5]). To generate the 100 MHz occupied transmission frequency bandwidth, the CP-OFDM waveform was generated using 120 kHz sub-carrier spacing and 69 resource blocks. Each resource block contains 12 subcarriers resulting in a total of 828 occupied sub-carriers. 16 QAM (Quadrature Amplitude Modulation) was used for data symbols and transmission length is 14 symbols which represent one new radio slot. Each transmission consists of 40998 bit of test data along with pilot and synchronisation symbols.

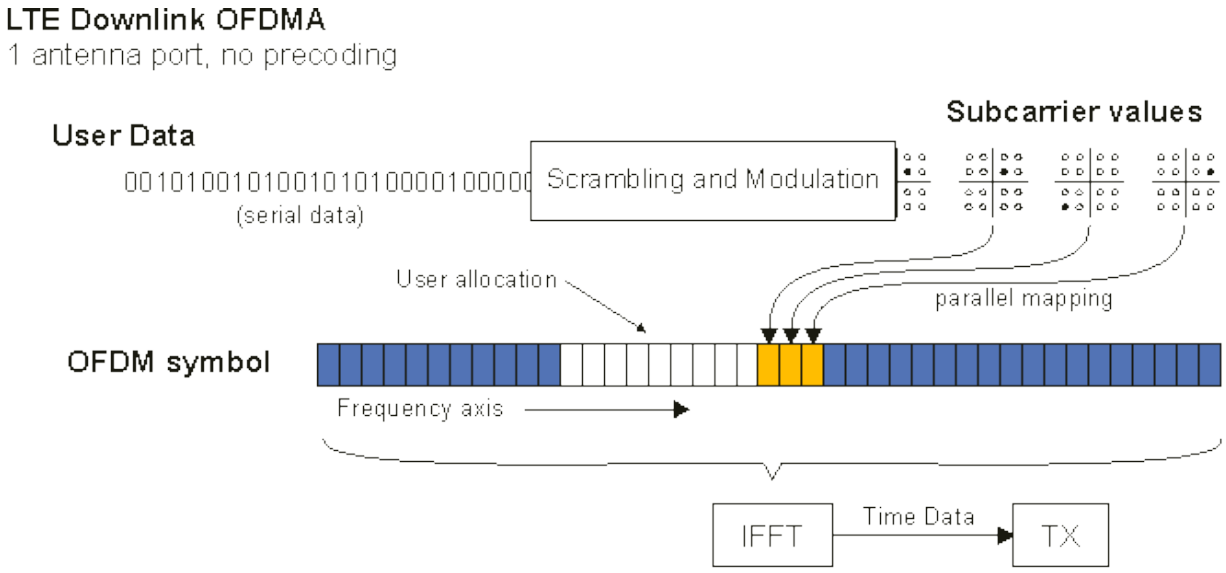

Figure 10 CP-OFDM data structure.

3.2.2 Waveform generation

Existing LTE code was used to insert pilot and synchronisation symbols at the transmitting end. This technique was employed to significantly reduce the amount of software development required to perform the testing. Three LTE sub-frames containing different payload data were generated and the symbols from the LTE resource grids were combined and inserted into the CP-OFDM resource grid as shown in Figure 11.

When the CP-OFDM waveform had been received and demodulated the resource grid is split back into three and processed as three separate LTE sub-frames where existing libraries could be used to equalise the received constellation. Synchronisation was provided by the MATE client using the 'Sync' option. The process to generate the waveform for transmission is as follows.

- Create three empty LTE resource grid.
- Generate random payload data to transmit and insert it into resource grids.
- Insert LTE synchronisation and pilot symbols into the resource grids. (only the pilots are currently used for equalisation of the received resource grids)
- Generate an empty CP-OFDM resource grid.
- Insert the symbols from the three LTE sub-frames into the CP-OFDM resource grid.
- Convert to resource grid to a waveform with CP-OFDM modulation and transmit through system.

The process detailed above is repeated for all desired and interference signals. Each transmission source contains random payload data.

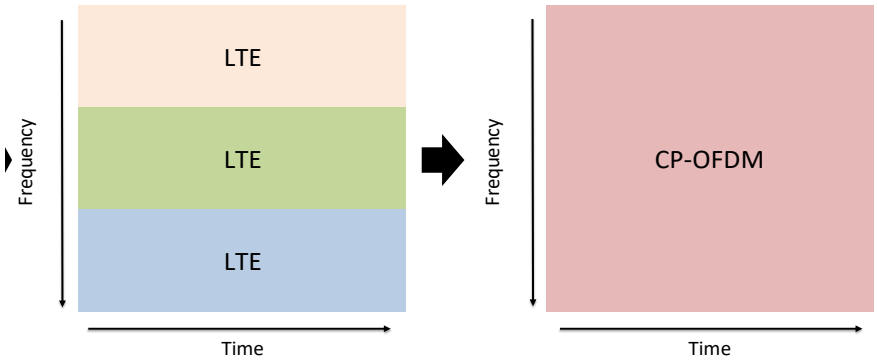

Figure 11 Layout of frame used during testing.

3.2.3 Waveform analysis

Existing LTE code was used to perform equalisation of the received symbols at the receiving end. The received CP-OFDM waveform is demodulated back into a resource grid. This resource grid is split into 3 LTE resource grids and these are then equalized using the pilot symbols contained within them. Error vector magnitude (EVM) and bit error rate (BER) quality metrics can then be calculated for all the data symbols received. A visualisation of the received CP-OFDM resource after it has been equalised is shown in Figure 12. The position of the symbols in the resource grid are shown in Figure 13.

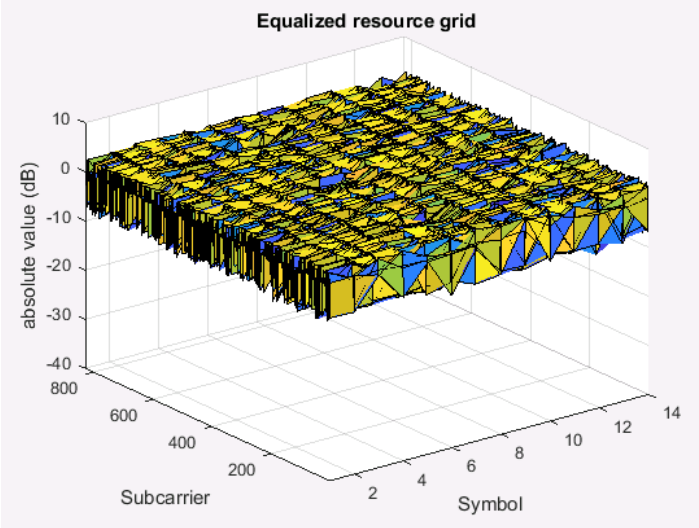

Figure 12 Diagram of received and equalised CP-OFDM resource grid.

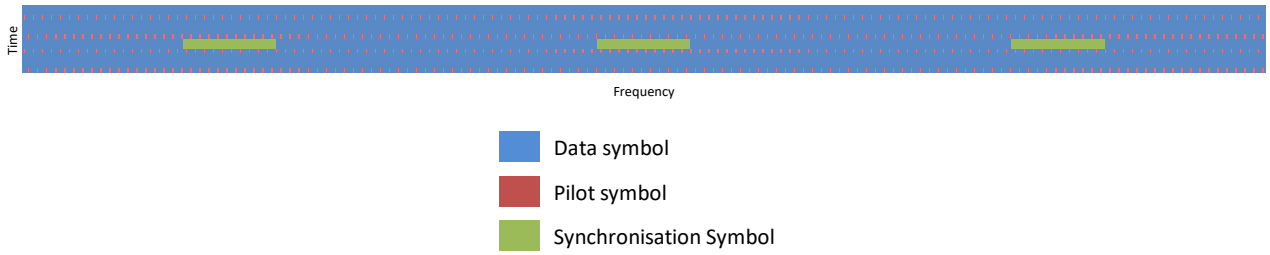

Figure 13 Diagram of CP-OFDM resource grid.

3.3 Measurement and Simulation setups

Figure 15 shows the measurement setup. The desired signal waveform is transmitted from one MATE antenna and any interference sources are transmitted from other antennas. In this work, the transmitted desired and interference signals are:

- either having the same centre frequency or different centre frequency
- either synchronised or non-synchronised in time.

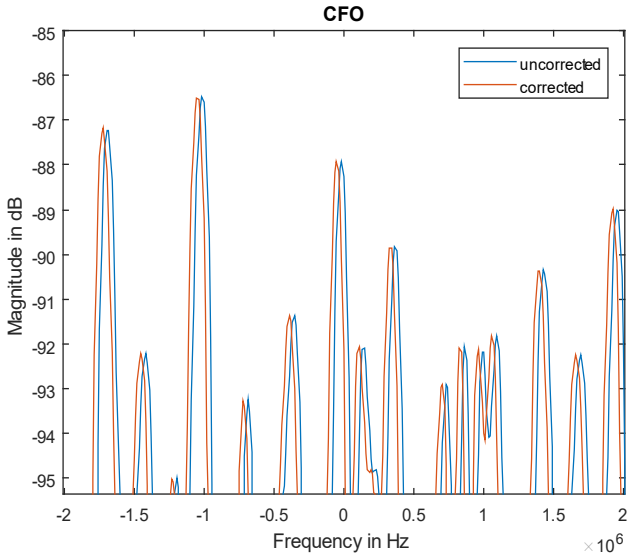

Figure 14 A plot of a subset of the received subcarriers showing the spectrum with and without CFO correction.

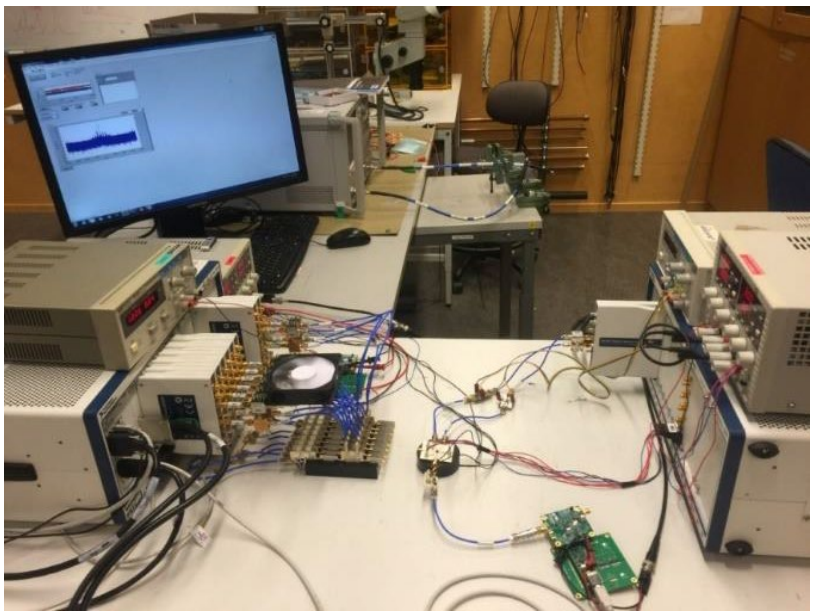

(a)

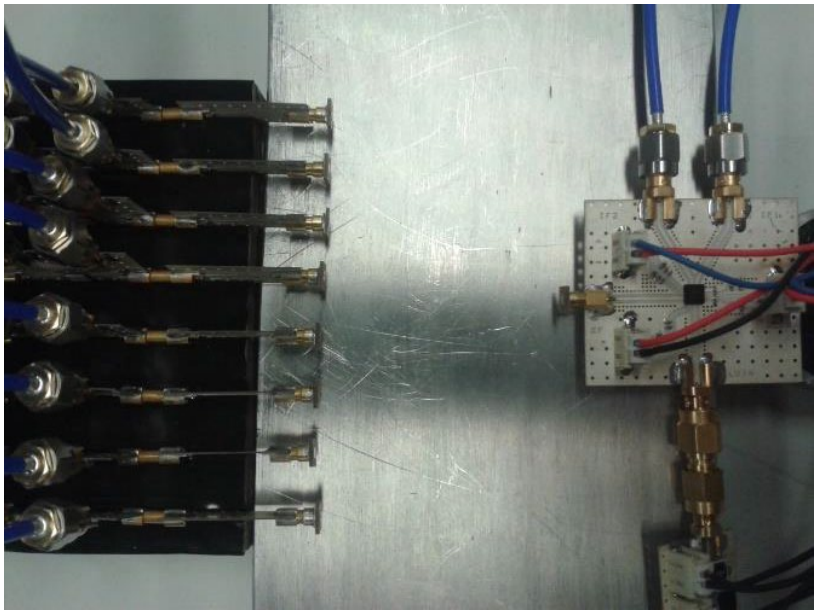

(b)

Figure 15 MATE Testbed measurement setup: (a) TXs on the left, RXs on the right; (b) Top view of TXs and Rx, the channel is in between.

The generated CP-OFDM waveform is frequency-shifted to + 150 MHz to avoid the mate hardware LO leakage and is then transmitted through either the MATE hardware or the MATE simulator. Once received the signal is shifted – 150 MHz and a software band pass filter (BPF) is applied to remove out of band interference, finally carrier frequency offset (CFO) correction is applied. This is illustrated in Figure 14.

3.4 Comparison between MATE and the MATE Simulator

This section presents the comparison between the performances of the MATE simulator and the MATE using different MATE simulators settings and the feedbacks associated with this study. Efforts to reduce this difference will be detailed in the following sections.

It should be noted that the MATE testbed is a dynamic testing environment. Antennas are moved around, hardware is changing, and temperature is variable. The MATE simulator, at the other hand, is more static. Thus, there is a need to calibrate the simulator to MATE at a certain point in time; at some other time, there will be discrepancies. Therefore, a first session of test has been performed where the simulator has been closely calibrated to the performance of MATE. For the rest of the tests, the simulator is the same, but the testbed is changing over time.

3.4.1 Measurements with a calibrated simulator

Here we present a few measurements, in time domain, frequency domain, and an I/Q plot, for a campaign where we first calibrated the simulator to produce similar results as MATE. We have chosen to transmit a single-carrier Quadrature Phase Shift Keying (QPSK) signal, at a bandwidth of 200 MHz. In Figure 16, we show the received time domain signal, in this case the I channel.

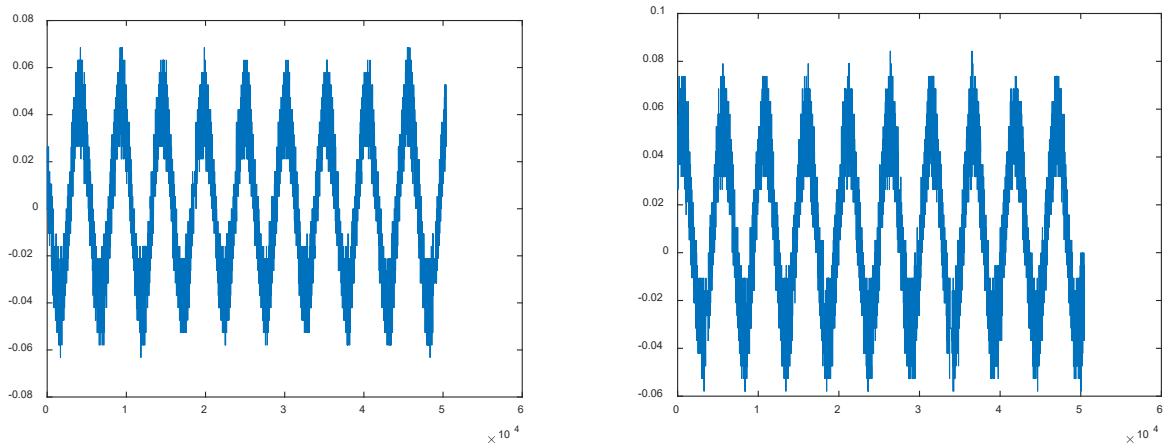

Figure 16 The received time domain signal (the I channel only) for the MATE testbed (left) and the simulator (right).

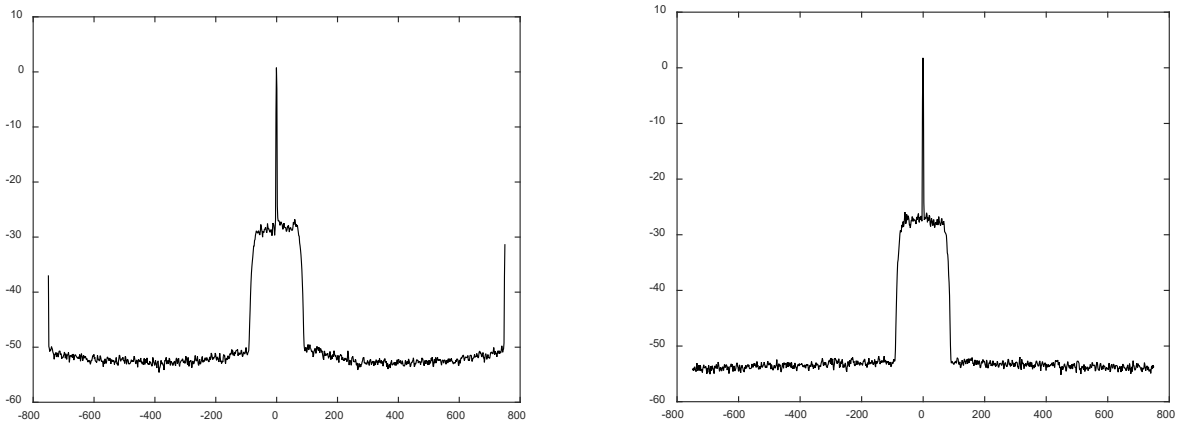

Figure 17 The received frequency domain signal for the MATE testbed (left) and the simulator (right).

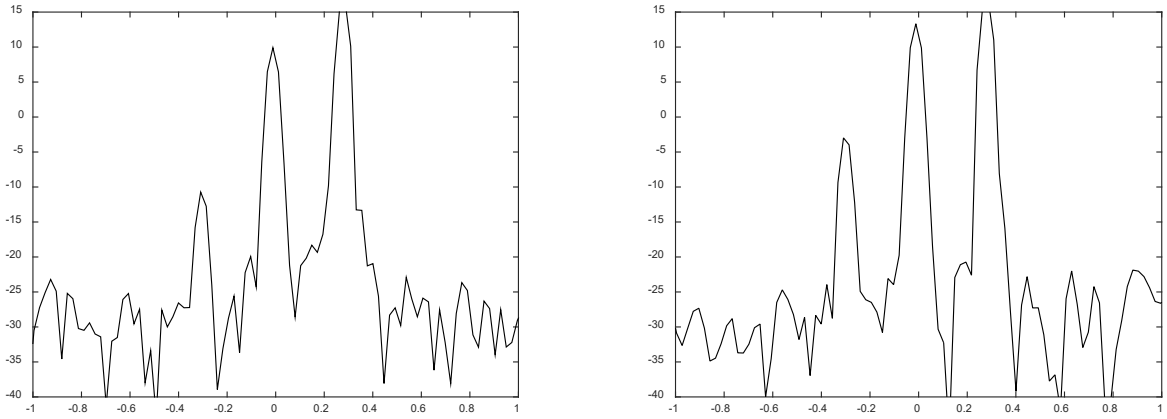

Figure 18 A zoomed-in version (from -1 to +1 MHz) of the spectrum for the MATE testbed (left) and the simulator (right).

We see a strong sinusoidal component, at around 300 kHz. This comes from an LO leakage component in the transmitter, and an offset between TX and RX LO frequencies of about 300 kHz. This leakage is very strong, actually stronger than the communication signal itself in this setting. The simulator faithfully reproduces this behavior, due to a preprogrammed offset and LO leakage in the same order as MATE. In Figure 17, we instead see the frequency domain signal corresponding to the same transmitted QPSK sequence. Similar to the time domain, the frequency domain shows a strong LO leakage close to the origin. In the zoomed-in frequency plot of Figure 18, we see that there are actually three components close to the origin.

In the zoomed-in plot, it is clear that we have a dominating component at +300 kHz, and its mirror (due to I/Q imbalance) at -300 kHz. We also have a DC (0 Hz) component, which stems from an LO leakage in the receiver circuitry. As in the time domain plots, also in the frequency domain the simulator is closely matching MATE. The largest differences are at the edges of the spectrum, where MATE has a strong spectral component which is not understood yet, and thus not part of the simulator. The I/Q plot in Figure 19 shows a few interesting things. This is as yet an unsynchronized received signal, directly measured at the output of the A/D converters.

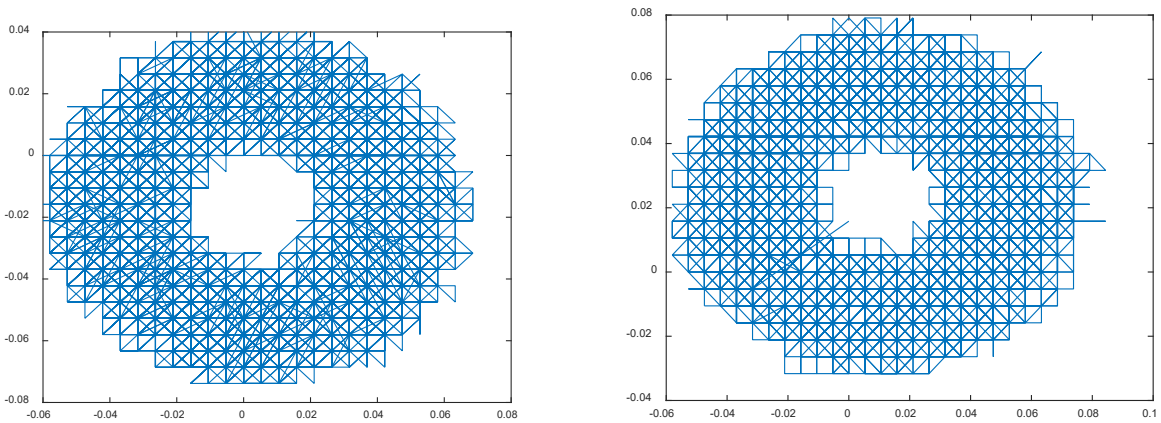

Figure 19 The I/Q plot for the MATE testbed (left) and the simulator (right).

First, we see an interesting donut shape. This is due to the TX LO leakage and the TX/RX frequency offset, which makes the entire I/Q diagram rotating around its center with 300 kHz. The

TX leakage creates DC offset at the transmitter, and the frequency offset makes it rotate. Second, we see a DC offset; the “donut” is not centered around the origin. This is due to the LO leakage at the RX side, creating a DC offset. In the simulator, this was also implemented.

3.4.2 Investigation on MATE simulator channel model

For investigating EVM and BER performance against SINR, two different CP-OFDM waveforms were generated to represent a desired signal and an interference source. The two waveforms were up-converted to shift the same centre frequency. Both signals were transmitted from different antennas as shown in Figure 20. The desired signal power was fixed for all measurements and the interference power level was adjusted in steps of 2 dB to produce varying SINR. The received channel power for the desired and interference signals were measured separately and then the EVM and BER were measured with both signals transmitting at the same time.

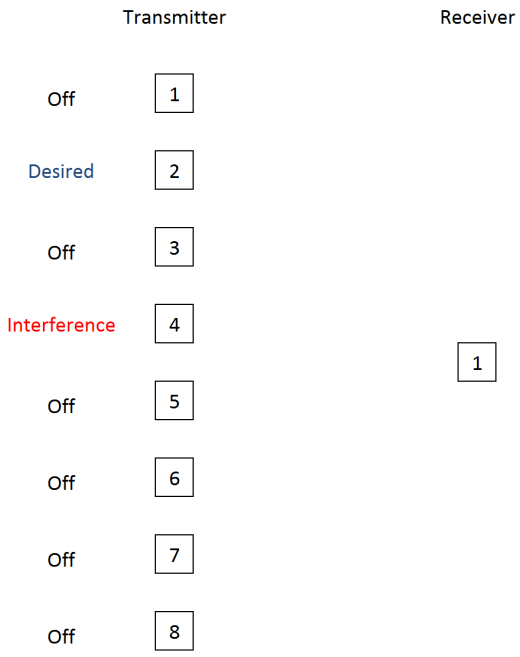

Figure 20 Schematic of MATE antennas used for measurements

The data transmission between the MATE hardware transmitting and receiving ends would be affected by their allocation hence the associated propagation channel response. i.e. changes in position of MATE antennas and surrounding objects will change the propagation channel response. To achieve comparable results between MATE and the MATE simulator must match the real system closely. Figure 21 and Figure 22 show the comparison of EVM and BER vs SINR without and with the use of correct propagation channel model in the MATE simulator. As depicted in Figure 21, there is a visible difference between the performance of MATE and the MATE simulator when incorrect propagation channel response is employed in the MATE simulator. Once the correct propagation channel response was employed into the simulator the improvement in the agreement between the MATE hardware and MATE simulator can be seen in Figure 22. Note that there is one outlining point visible on both EVM and BER plots for the MATE testbed results. This is the result of a single transmission that was not received correctly. The results obtain here form MATE will be compared to the MATE simulator in the flowing sections.

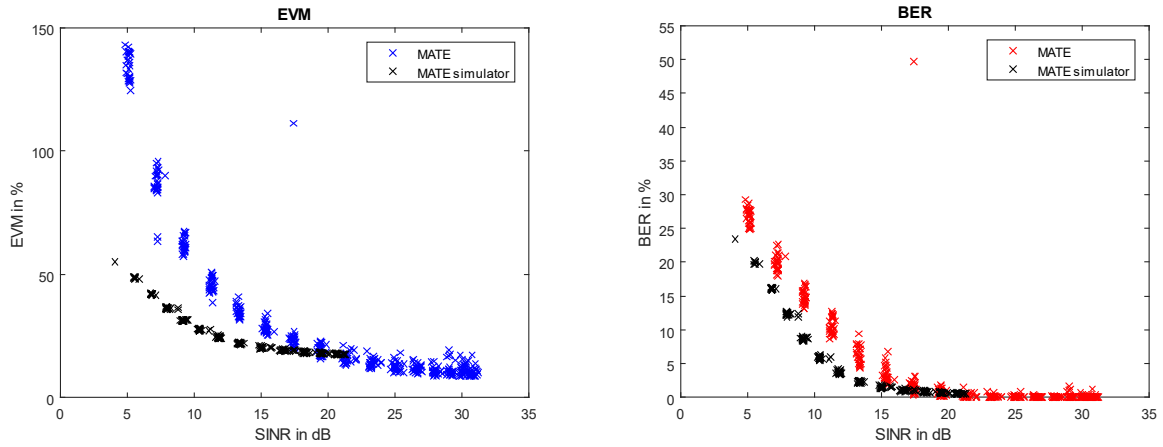

Figure 21 Comparison of EVM (left) and BER (right) between MATE and the MATE simulator without using the correct propagation channel matrix in the MATE simulator.

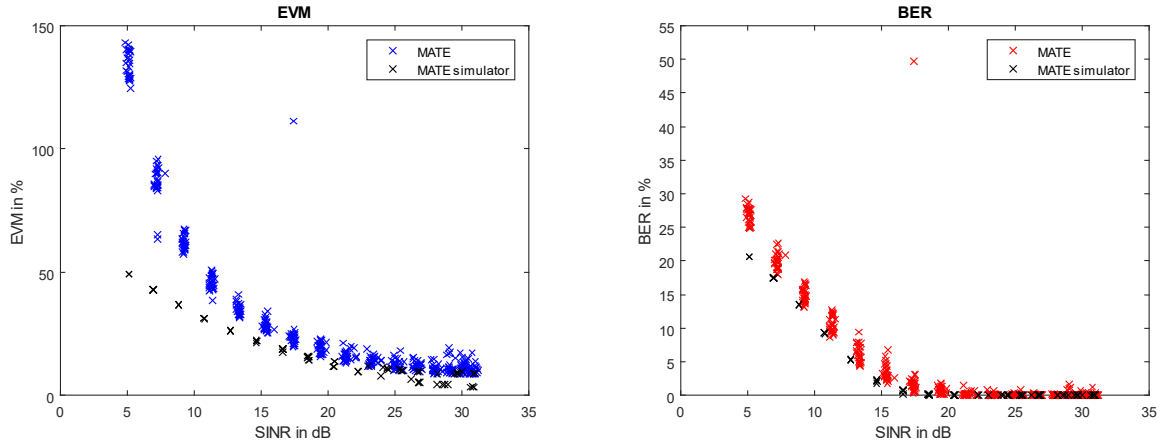

Figure 22 Comparison of EVM (left) and BER (right) between MATE and the MATE simulator after using the correct propagation channel matrix in the MATE simulator.

3.4.3 Comparison for Constellation Diagram and Received Spectrum

Without considering interference, this subsection presents a comparison for constellation diagram and received spectrum between MATE and MATE simulator. The same data was transmitted through MATE and the MATE simulator. Figure 23 and Figure 24 show the constellation diagram and the received frequency spectrum for MATE and the MATE simulator.

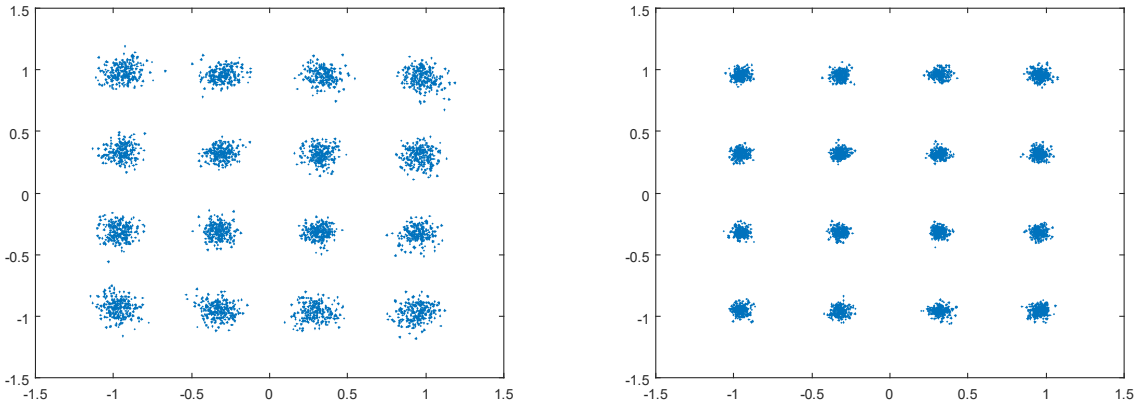

Figure 23 Demodulated constellation of MATE (left) and MATE simulator (Right) when using a single desired signal.

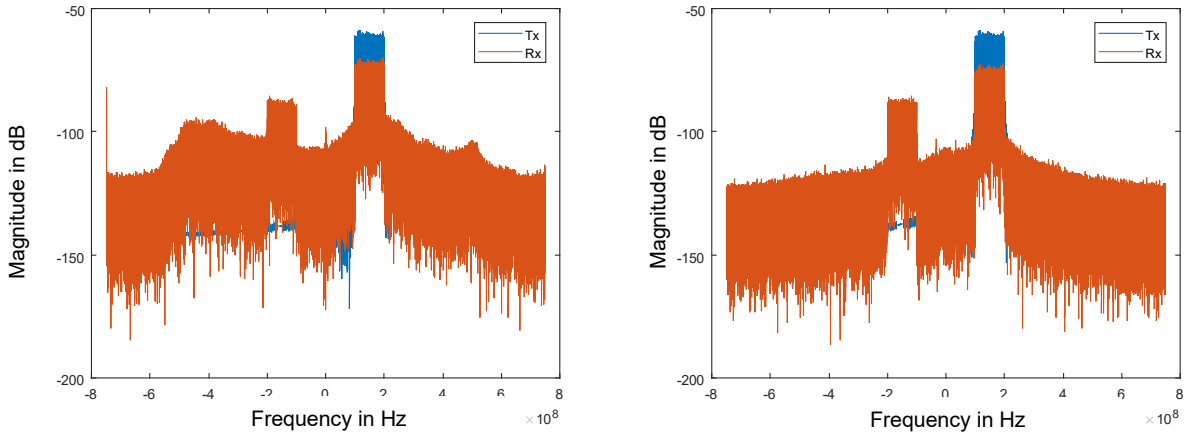

Figure 24 Received spectrum of MATE (left) and MATE simulator (Right) when using a single desired signal.

3.4.4 Investigation on adjustments to the simulator noise floor

During the second set of simulator runs is was observer that the noise floor of the physical MATE system was higher than the simulator as shown in Figure 25. The simulator contains parameters to control all aspects of the simulation. The noise floor was adjusted and the simulation was repeated. Figure 26 shows the results of the simulator with the adjusted noise floor compared to the MATE measurements. This has reduced the maximum SINR as the noise level is now higher.

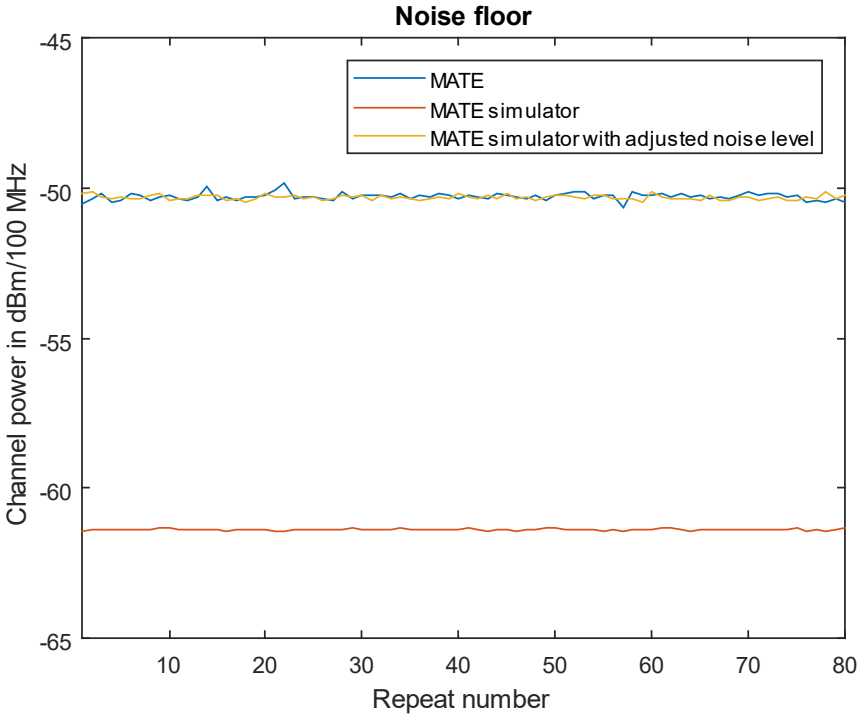

Figure 25 Noise floor measurement of MATE and the MATE simulator, showing the initially and updated simulated level.

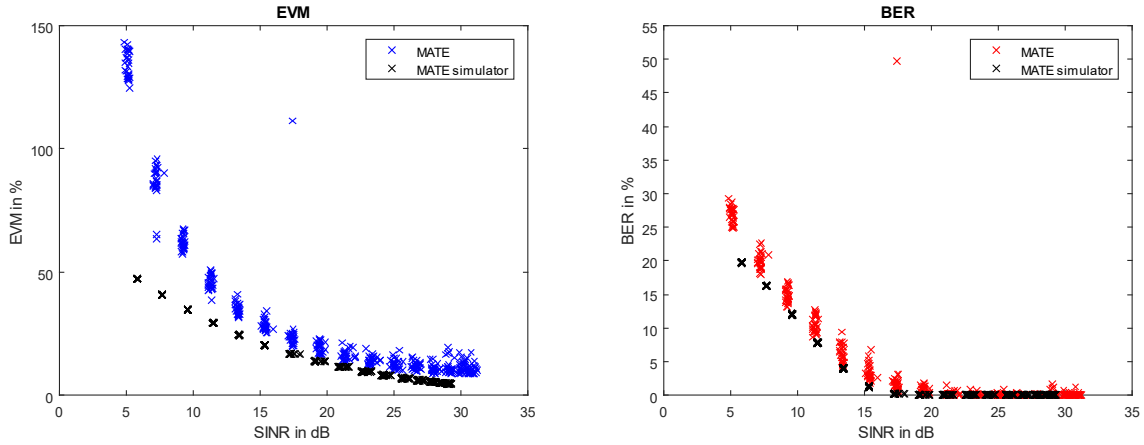

Figure 26 Comparison of EVM (left) and BER (right) between MATE and the MATE simulator after the noise level of the simulator had been adjusted to match the simulator.

3.5 Further investigations using the MATE simulator

In this subsection, the MATE simulator was used to investigate a number of distortion sources by intentionally adjusting software parameters.

3.5.1 Carrier frequency offset

It is possible to see the influence of incorrect CFO correction by forcing an incorrect value. In Figure 27 the constellations for a signal transmitted using the simulator with offsets forced to 0 Hz, + 50 Hz and + 100 Hz are shown with resulting EVM of 5.7%, 8.2% and 11.6% respectively.

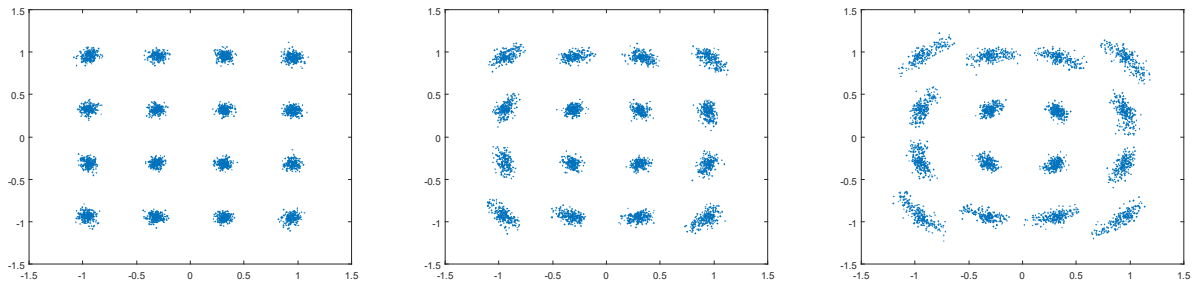

Figure 27 Simulator run with an intentional carrier frequency offset (CFO) for the desired signal only. Shows no offset (Left), + 50 Hz offset (Centre) and + 100 Hz offset (Right).

3.5.2 Synchronisation failure

By disrupting the synchronisation preamble it is possible to disrupt the synchronisation process. A comparison between a correct and failed synchronisation is shown in Figure 12.

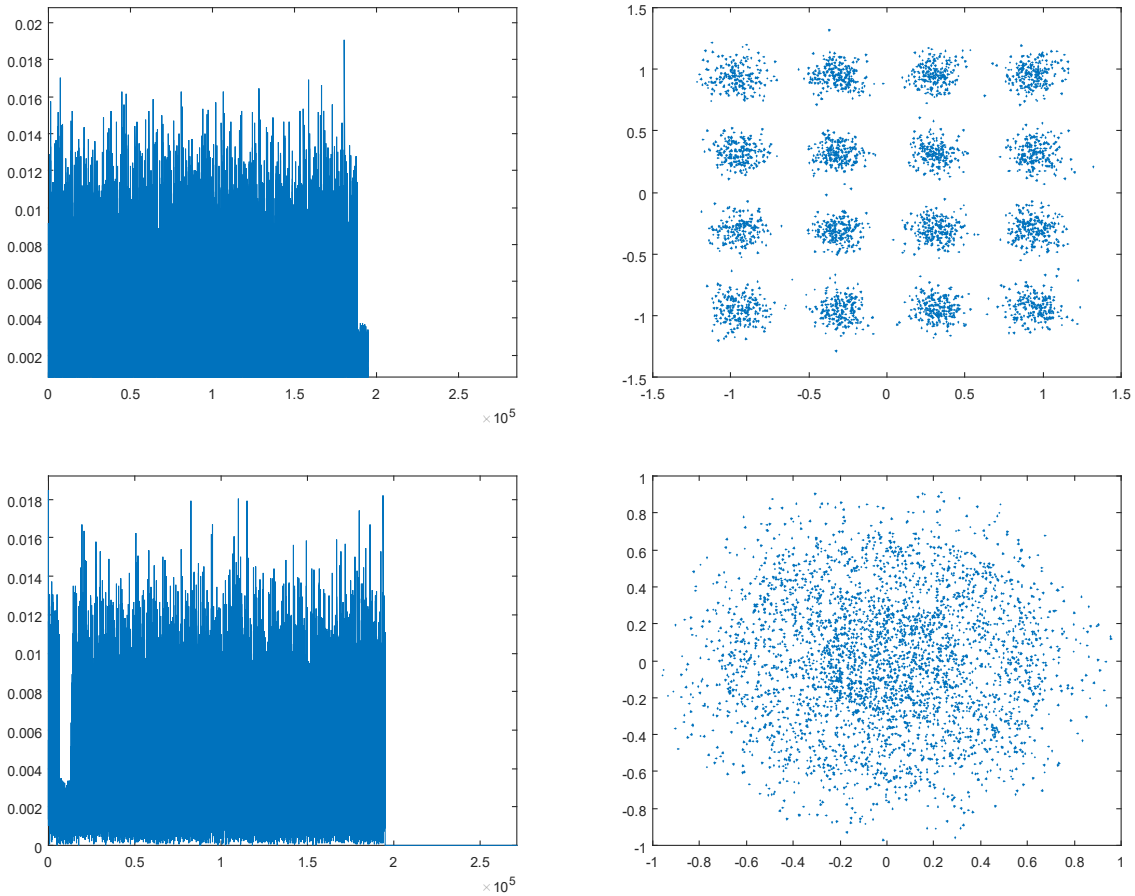

Figure 28 Time domain waveform magnitude (left) and constellation diagram (right) for a frame with correct (top) failed synchronisation (Bottom).

3.5.3 Investigation on an in-band interference source

In this subsection, the constellation diagram (see Figure 29) and the received power spectrum (Figure 30) for the scenario where both the interference and desired signals are in the same band. The constellation diagram results show the relevant issues introduced by the inter-user interference. The received power spectrum show in Figure 30. As depicted in the received power spectrum plot in Figure 30, the Rx RF signal has an attenuated image at lower sideband.

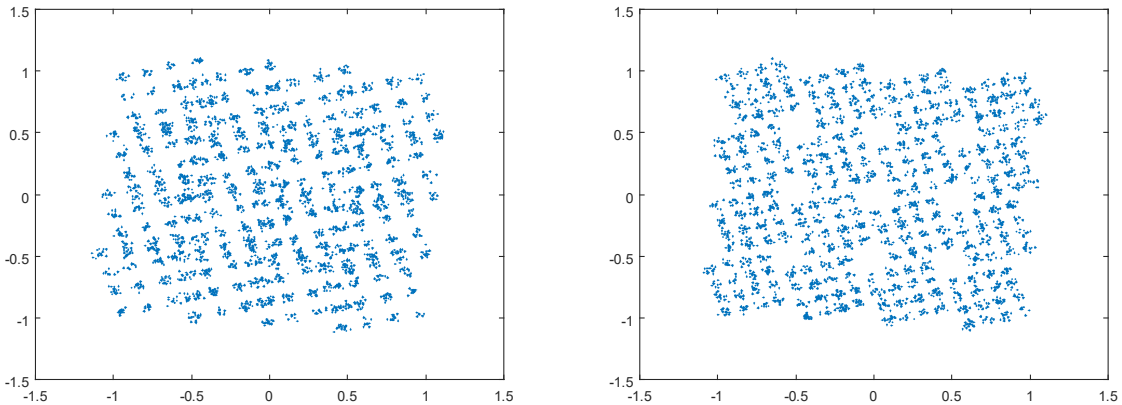

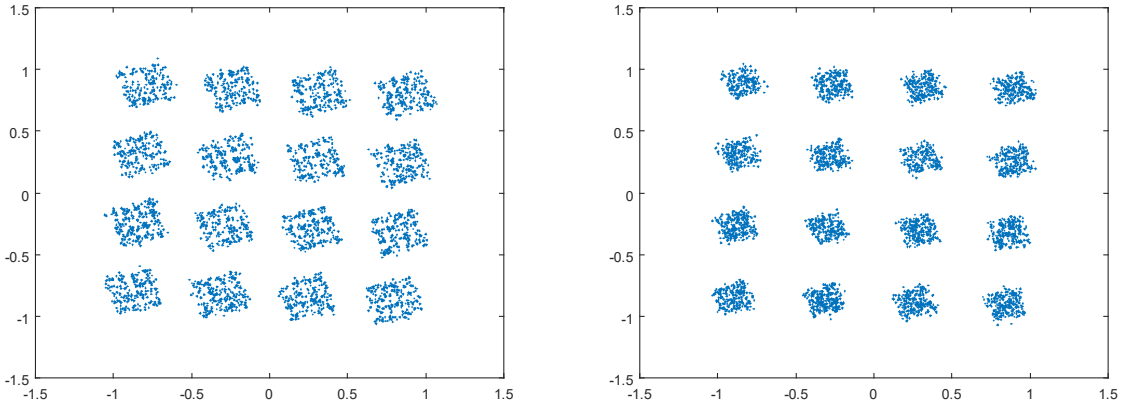

Figure 29 Constellation diagrams for: left to right and top to bottom, represent increasing SINR.

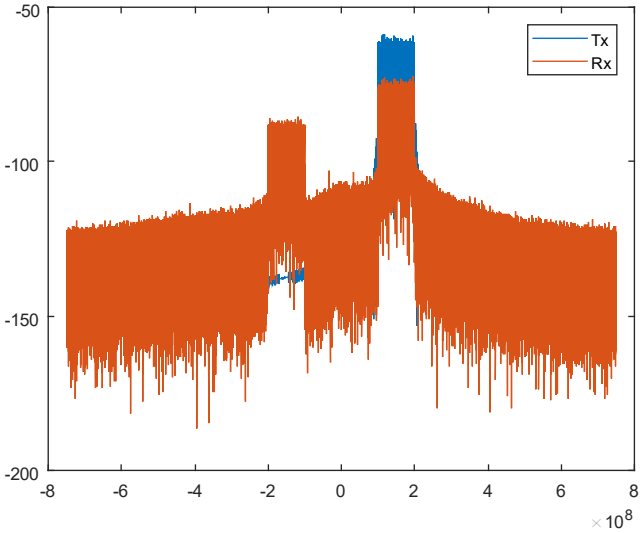

Figure 30 Received Power Spectrum.

3.5.4 Investigation on an out-of-band interference source

In this subsection, the interference signal is in an adjacent band to the desired signal. The desired signal is centred at +150 MHz and the interference signal is centred at +250 MHz, each of the signals occupies a 100 MHz wide band.

Simulator EVM, SINR does not change by much in this configuration as very little power is leaking from the interference to the desired channel. This looks like a signal to noise measurement (see Figure 31).

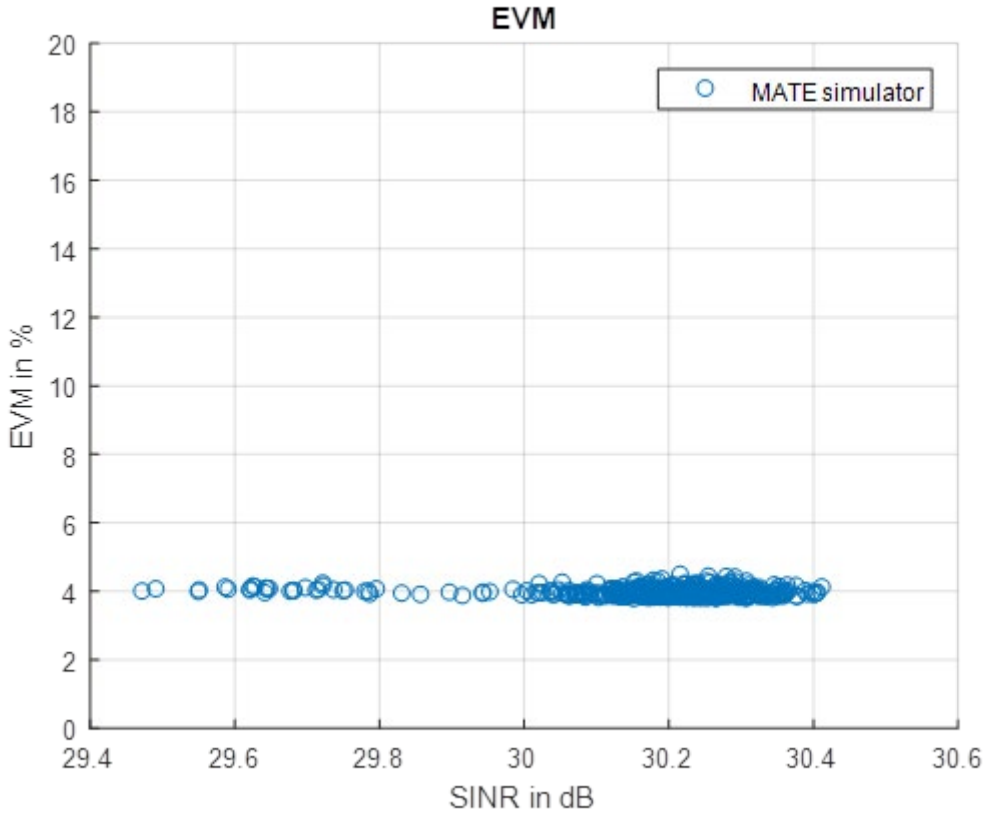

Figure 31 EVM vs SINR for the MATE simulator with an adjacent channel interference source.

The power spectrum of the signal transmitted is shown in Figure 32.

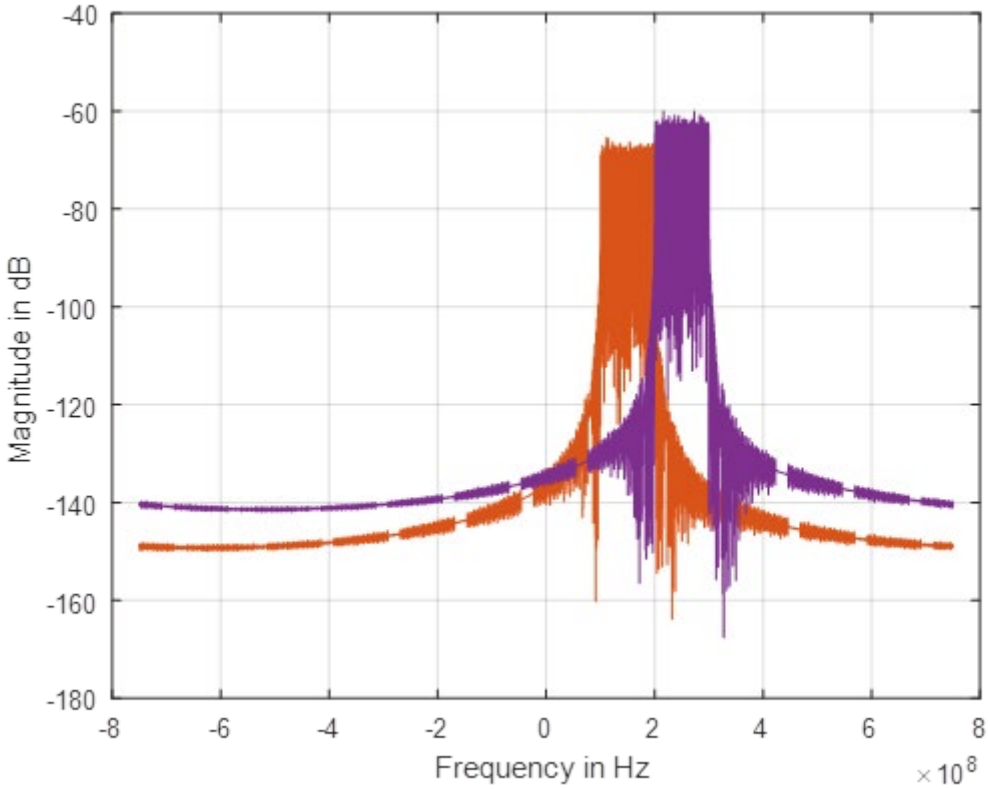

Figure 32 Transmitted power spectrum for the adjacent channel interference testing. The desired signal is shown in red and the interference signal is shown in purple.

The received power spectrum and desired signal power spectrum are shown in Figure 33. Note that the power level of the interference signal is now lower due to the different propagation paths from each transmit antenna to the receiver.

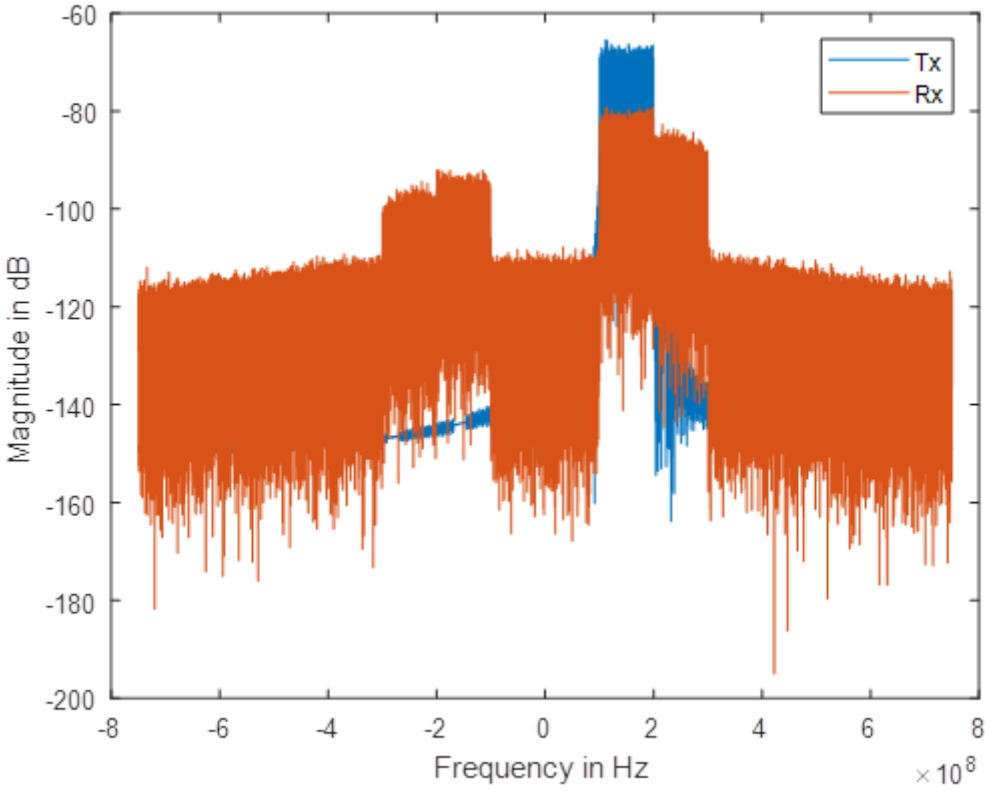

Figure 33 Simulated received and transmitted power spectrum for the MATE simulator. Note that only the desired transmitted signal is shown.

4 Analysis of data findings and Verification of the SINR definition

4.1 Measurement Campaign (1)

The ultimate purpose of the measurements detailed in section 2.2 was to ascertain what impact frequency selective wideband channels would have over the prediction error when estimating SINR. The prediction error is defined in decibels as the difference between the actual SINR with signaling using the transmission waveform and the predicted SINR based on the measured EVM. Therefore the prediction error should ideally be 0 dB. The degree of prediction error due to wideband channel fading is dependent on two factors:

1. The bandwidth of the waveform over which the pilot is transmitted to estimate the SINR. It must be substantially narrower than the bandwidth over which the SINR is coherent in the channel.
2. The degree of quadrature amplitude modulation (QAM) used in the waveform. It was found from earlier simulations using synthetic data in D1 that it is necessary to use a modulation scheme whereby there is a minimum of 32 QAM. Using smaller constellations will not generate interference that is resembling of Gaussian additive noise and will cause a reduction in prediction error.

In the experimentation carried out, 64 QAM was used to exceed the requirement in 2 above, but the measurements would determine how wide the bandwidth could be to enable the SINR to be reliably predicted based on the root mean square (RMS) EVM, which was evaluated over the whole bandwidth and time interval, thus some carries within the band may have considerably different EVM to others, which would affect the overall RMS value. Therefore a higher prediction error occurs with an increase in bandwidth. Both the mean and standard deviation on the prediction error were evaluated over the whole channel and plotted vs bandwidth shown in Figure 34. Clearly bandwidths between 2 MHz and 5 MHz are within the coherence of the SINR of the channel to allow a low standard deviation on the prediction error, while increasing the bandwidth substantially worsens this in all three scenarios, reaching a higher error for Rx6 Spatial than Rx3 Spatial due to the wider frequency selectivity of that channel going beyond bandwidths where the actual SINR is coherent.

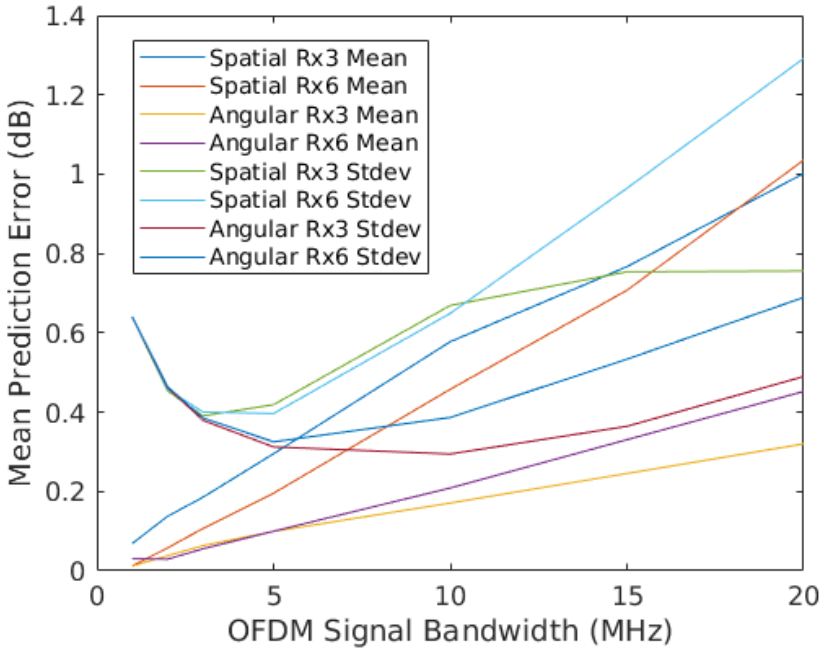

Figure 34 Final result evaluating the mean and standard deviation on the prediction error for the three measured scenarios.

The Rx3 Angular case has similar characteristics to the Rx3 Spatial as would be expected case due to the antennas being in close proximity but there is more time variance as well. An interesting observation is that a very narrowband waveform of 1 MHz has a higher standard deviation than 2 MHz for all cases. This could be explained by the fact that narrower bandwidth results in a smaller number of carriers, which causes greater uncertainty in the RMS EVM with an insufficient set of samples within the 20 frames over which it was evaluated. An increased number of sub-carriers over wider bandwidths enables a sufficient sample size to obtain a 'more true' RMS EVM.

The results presented in this work have verified that the EVM has the ability to predict SINR if the waveform has a transmission bandwidth is within the coherence bandwidth of the channel's SINR. A further important assumption is the assumption that the wanted signal is transmitting a sufficient number of frames with a QAM order above 32 QAM to evaluate the RMS EVM and that the interfering signals are of suitably high modulation order and have consistent transmission across the bandwidth of the waveform that they can be modelled as Gaussian white noise. Such conditions would not hold if for example the side band interference of a waveform was being analysed since there would be frequency variance in the noise or that the QAM order was too low. Additionally it

has to be assumed the interference delivery is constant.

Not accounted for in this campaign is the non-linear effects of the transmitter. Due to the peak to average power ratio (PAPR) of the OFDM being transmitted, even with back off at the transmitter the non-linear effects will cause some intermodulation distortion which will create some peak EVM even with a high SINR at the receiver. Such evaluations have to be taken into account with a real device over which such data is being analysed, which are difficult to evaluate in a reliable way theoretically.

4.2 Measurement Campaign (2)

The results presented in this section details SINR tests performed with both testbeds operating in MIMO mode (see Figure 35 and Figure 36). MATE used all of the available transmit antennas to transmit a single frame using beamforming. The NPL system was used as an interference source and was transmitting unique frames on both of the transmit antennas, mimicking the signals it generates to achieve spatial multiplexing.

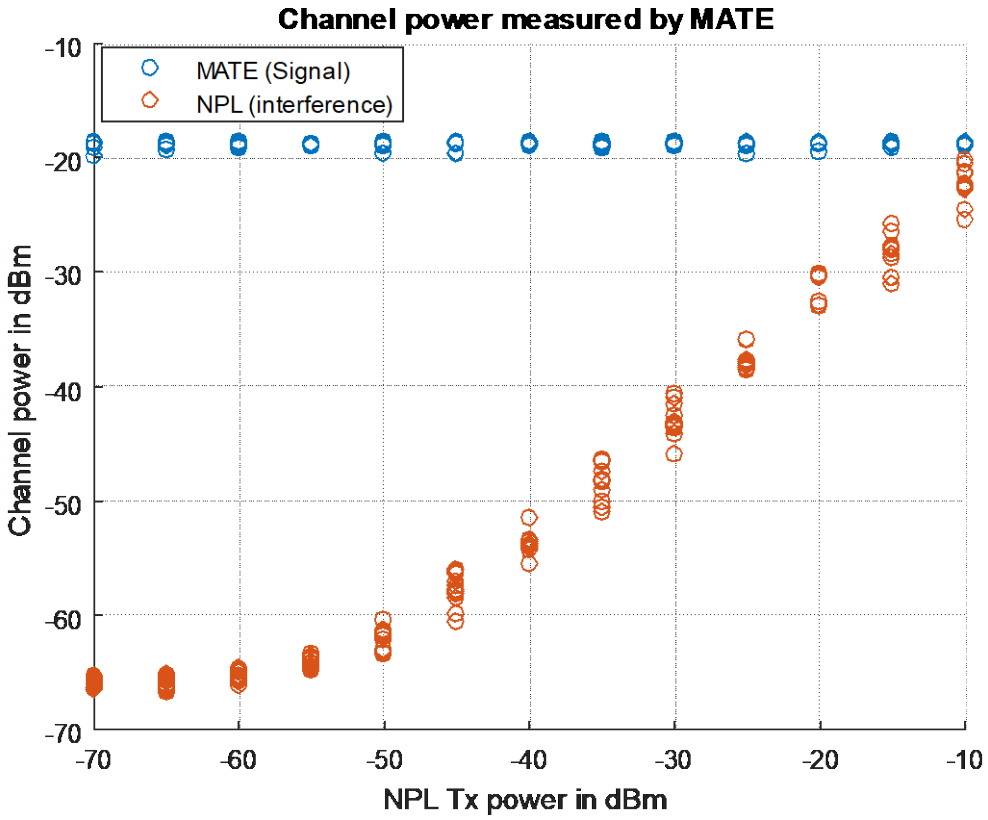

Figure 35 Measured Channel Power for MIMO operation using MATE receiver. Note that, in total 173 measurements were made at 13 interference transmit power levels.

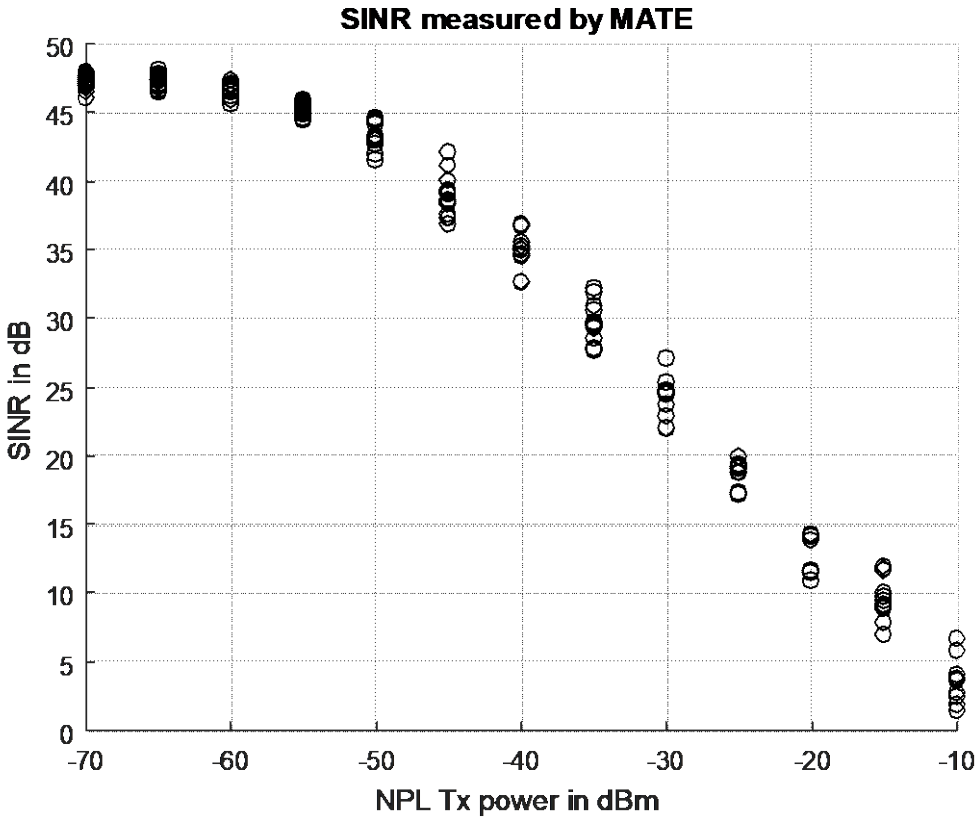

Figure 36 Calculated SINR using the channel power measured by the MATE receiver.

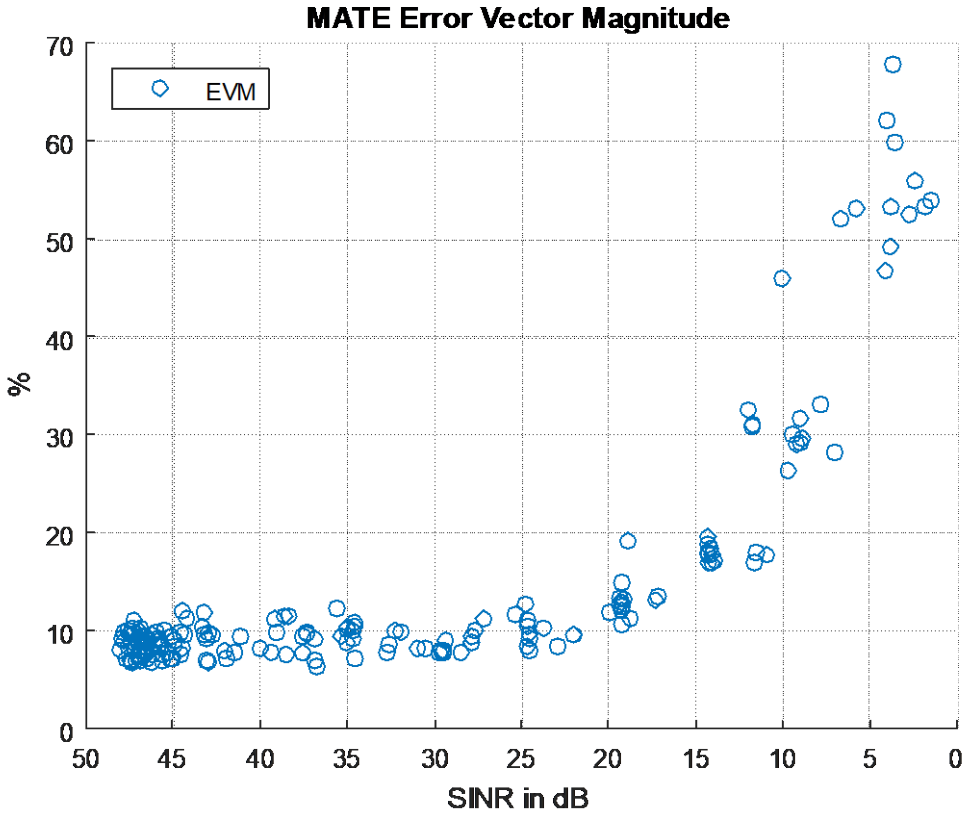

Figure 37 EVM for the frames transmitted through MATE.

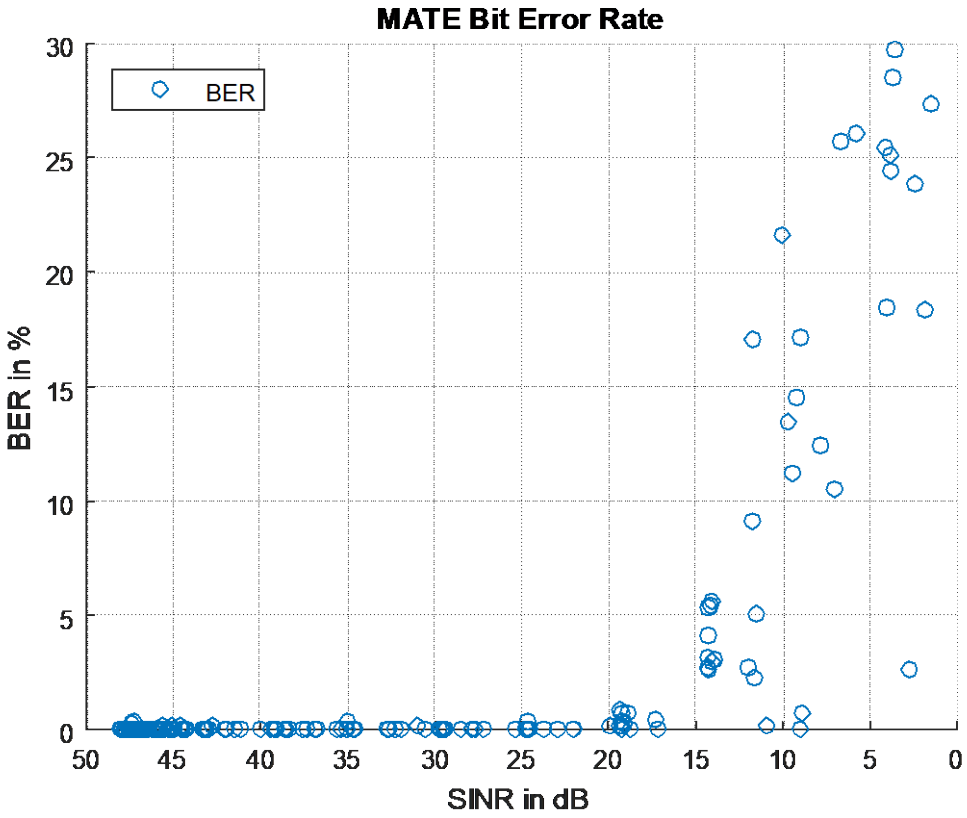

Figure 38 BER for the frames transmitted through MATE.

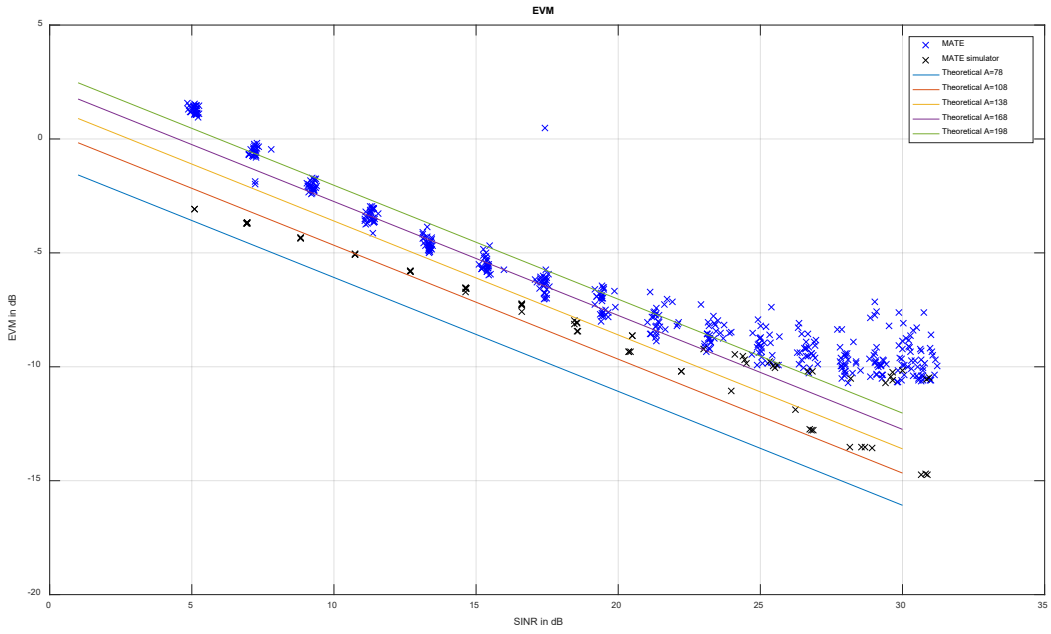

Figure 39 A comparison of EVM for the frames transmitted through MATE, MATE simulator and the predicted SINR.

Figure 37 and Figure 38 show the measured EVM and BER results, respectively. The received signal from MATE has increased by more than 10 dB when compared to operation in SISO mode [4]. This is partially as a result of the beamforming gain achieved when using multiple transmit

antennas. Note that this exceeds the expected theoretical increase of 9.0 dB due to beamforming of 8 antennas alone. The theoretical increase is only expected to be seen when all transmit powers are equal and all paths to the receiver are equal. Since the power levels at each TX are not exactly equal, and the individual paths from the individual TX to the RX differ, a slightly higher beamforming gain is found. Figure 39 shows a comparison of EVM for the frames transmitted through MATE, MATE simulator and the predicted SINR as defined in Equation (2) where different value of A was explored. This is to investigate how its change effects the fitting to the practical measurement and hence the SINR definition.

5 Conclusion

In this work, we have reported: 1) a comparison of MIMO SINR performance for measurement campaigns (1) and (2); 2) feedback to software simulator for in-band and out-of-band scenarios; and 3) verifying and applying changes to SINR definition for 5G communication, where applicable. A 5G waveform candidate has been employed. Based on the measurement findings, the SINR definition has been assessed and validated in this report.

6 References

[1] T. Brown, D. Humphreys, M. Hudlika, and M. Dieudonne, "Definition of SINR - MIMO, under 14IND10 MET5G A1.1.3," May 2017.

[2] D. Humphreys, T. Brown, and M. Hudlika, The performance characteristics of SINR definitions suitable for 5G communication, Validation Report, 14IND10 MET5G D1, Mar. 2018.

[3] E. G. Larsson, O. Edfors, F. Tufvesson and T. L. Marzetta, "Massive MIMO for next generation wireless systems," *IEEE Communications Magazine*, Vol. 52, No. 2, pp. 186 – 195, Feb. 2014.

[4] K. Buisman, T. Eriksson, T. H. Loh, D. Cheadle, M. Wang, D. Humphreys, T. Brown, and M. Dieudonne, SINR performance for interferences originating within and external to the massive MIMO testbed suitable for 5G communication, Evaluation Report, 14IND10 MET5G D3, Jan. 2018.

[5] Website: Available at http://rfmw.em.keysight.com/wireless/helpfiles/89600b/webhelp/subsystems/lte/content/lte_overview.htm